Meteoritics & Planetary Science 39, Nr 7, 1199–1221 (2004)
Abstract available online at http://meteoritics.org

Hydrothermal alteration in the core of the Yaxcopoil-1 borehole, Chicxulub impact structure, Mexico

Lukas ZÜRCHER* and David A. KRING

Lunar and Planetary Laboratory, University of Arizona, 1629 East University Boulevard, Tucson, Arizona 85721, USA
*Corresponding author. E-mail: lzurcher@geo.arizona.edu

(Received 3 September 2003; revision accepted 31 March 2004)

Abstract–Petrographic, electron microprobe, and Raman spectrometric analyses of Yaxcopoil-1 core samples from the Chicxulub crater indicate that the impact generated a hydrothermal system. Relative textural and vein crosscutting relations and systematic distribution of alteration products reveal a progression of the hydrothermal event in space and time and provide constraints on the nature of the fluids. The earliest calcite, halite, and gaylussite suggest that the impactite sequence was initially permeated by a low temperature saline brine. Subsequent development of a higher temperature hydrothermal regime is indicated by thermal metamorphic diopside-hedenbergite ($Aeg_3Fs_{18–33}En_{32–11}Wo_{47–53}$) after primary augite and widespread Na-K for Ca metasomatic alkali exchange in plagioclase. Hydrothermal sphene, apatite, magnetite ± (bornite), as well as early calcite (combined 3 to 8 vol%) were introduced with metasomatic feldspar. A lower temperature regime characterized by smectite after probable primary glass, secondary chlorite, and other pre-existing mafic minerals, as well as very abundant calcite veins and open-space fillings, extensively overprinted the early hydrothermal stage. The composition of early and late hydrothermal minerals show that the solution was chlorine-rich (Cl/F >10) and that its Fe/Mg ratio and oxidation state increased substantially (4 to 5 $\log fO_2$ units) as temperature decreased through time. The most altered zone in the impactite sequence occurs 30 m above the impact melt. The lack of mineralogical zoning about the impact melt and convective modeling constraints suggest that this unit was too thin at Yaxcopoil-1 to provide the necessary heat to drive fluids and implies that the hydrothermal system resulted from the combined effects of a pre-existing saline brine and heat that traveled to the Yaxcopoil-1 site from adjacent areas where the melt sheet was thicker. Limonite after iron oxides is more common toward the top of the sequence and suggests that the impactite section was subjected to weathering before deposition of the Tertiary marine cover. In addition, scarce latest anatase stringers, chalcopyrite, and barite in vugs, francolite after apatite, and recrystallized halite are the likely products of limited post-hydrothermal ambient-temperature diagenesis, or ocean and/or meteoric water circulation.

INTRODUCTION

This paper presents the results obtained thus far in our ongoing research into the origin and evolution of the post-impact hydrothermal system in the Chicxulub crater. Impact-generated fluid regimes can encompass large volumes of the Earth's crust. At the Siljan impact crater, drilling and surface sampling indicate hydrothermal fluids affected the entire 52 km diameter of the structure down to a depth of at least 1.2 km (Komor et al. 1988). In the larger Puchezh-Kantunki crater (80 km diameter), the hydrothermal system is known to extend to a depth of at least 5 km (the bottom of the Vorotilovskaya borehole) in the uplifted peak in the center of the impact structure (Pevzner et al. 1992). Post-impact hydrothermal activity has also been recognized at the Kärdla (4 km in diameter; Versh et al. 2003), Haughton (24 km in diameter; Bain et al. 1988; Osinski et al. 2001), Manson (35 km in diameter; Boer et al. 1996; McCarville and Crossey 1996), Saint Martin (~40 km in diameter; Simonds and McGee 1979; Reimold et al. 1990), and Sudbury (~250 km in diameter; Grieve and Masaitis 1994; Therriault et al. 1999) impact craters. In addition, degassing of volatiles from impact breccias has been described at the Ries crater (24 km in diameter; Newsom et al. 1996). The hydrothermal system at Chicxulub (~180 km in diameter) may be one of the most extensive and best-preserved for study.

Impact-related hydrothermal systems are important because fluid processes influence the thermal (e.g., Abramov

and Kring 2003) and chemical evolution of an impact crater. Compositions and crosscutting relations of hydrothermal alteration products can provide constraints on the relative timing and nature of the pre-hydrothermal setting of the crater, the fluid regime that followed, and post-hydrothermal weathering and diagenesis. Hydrothermal alteration products can also be used to estimate the temperature gradient and its evolution with time in different parts of the crater. Furthermore, hydrothermal fluids are known to be consequential in the formation of economic mineral deposits (i.e., Sudbury; Ames et al. 1998), and may have played an important role in the origin and evolution of early life (Kring 2000a, b). In addition, filtering out the effects of metasomatism is essential to deduce the original composition of an altered impact melt and the character of the sampled crust.

Post-impact hydrothermal alteration was first noted at Chicxulub in the Yucatán-6 borehole located ~50 km from the center of the structure (Kring et al. 1991; Kring and Boynton 1992; Schuraytz et al. 1994; Gonzalez-Partida 2000). In 2001–2002, continuous core was recovered from the Yaxcopoil-1 borehole drilled ~60 km from the center of the structure (Kring et al. 2004, and other papers from this issue). This new core also showed extensive hydrothermal alteration (Ames et al. 2003; Hecht et al. 2003; Lüders et al. 2003; Zürcher and Kring 2003; Zürcher et al. 2003) and substantiated the idea that the hydrothermal system at Chicxulub may be continuous and rather large.

Six units were originally logged within the impactite sequence at Yaxcopoil-1 (Dressler et al. 2003). These authors tentatively described these units from top to bottom as redeposited suevite (unit 1: 13.39 m thick), suevite (unit 2: 14.86 m thick), chocolate-brown melt breccia (unit 3: 22.94 m thick), variegated and glass-rich suevitic breccia (unit 4: 15.26 m thick), green monomict autogene melt breccia (unit 5: 23.86 m thick), and variegated polymict allogenic-clast melt breccia (unit 6: 10.02 m thick). This study contributes new results obtained from a detailed examination of hydrothermal replacement textures, vein crosscutting relations, and mineral compositions observed in 16 samples collected from unit 1 through unit 5. From top to bottom, samples are identified by the depth in meters from where they were collected: Yax-1_800.43 from unit 1; Yax-1_813.41, Yax-1_819.83, and Yax-1_821.76 from unit 2; Yax-1_828.68, Yax-1_829.56, Yax-1_832.83, Yax-1_836.34, and Yax-1_841.32 from unit 3; Yax-1_857.65 from unit 4; Yax-1_861.40, Yax-1_863.51, Yax-1_867.76, Yax-1_872.32, Yax-1_876.46, and Yax-1_883.13 from unit 5. Relative sample locations are depicted in Fig. 1. Because hydrothermal products are systematically distributed in space and time, we were able to deduce several aspects about the primary composition of the impact melt unit, permeability, probable pre-hydrothermal paleogeographic setting, origin and evolution of the hydrothermal system, and extent of post-hydrothermal processes.

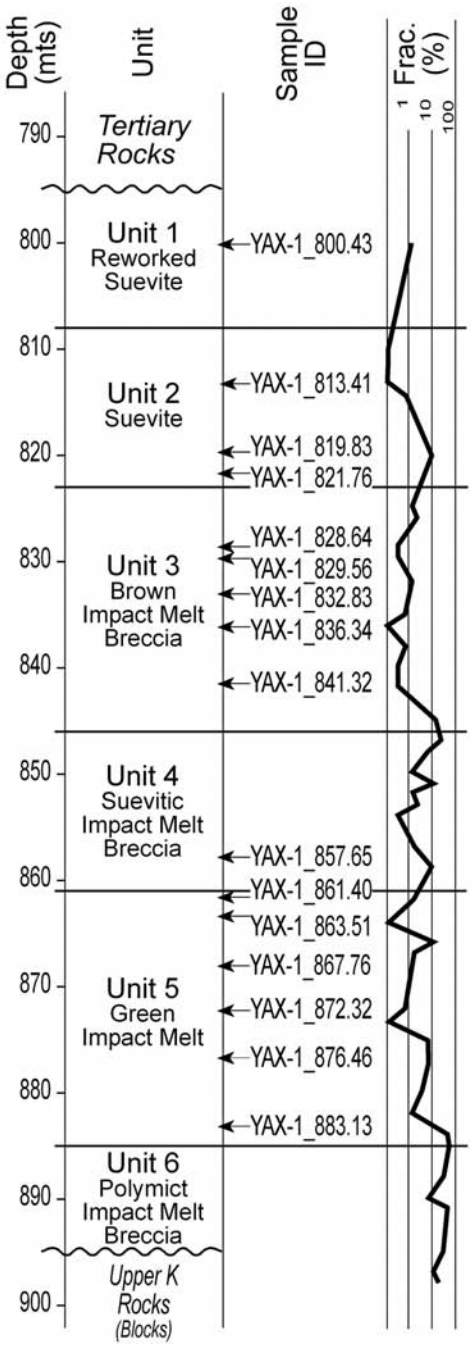

Fig. 1. Relative position of studied samples in the Yaxcopoil-1 impactite section and estimated fracture densities in the core.

METHODOLOGY

In this study, we applied techniques traditionally used in ore deposit research. We obtained fracture density estimates by visual inspection of scanned color images of the Yaxcopoil-1 core. We used thin section petrography and backscattered electron (BSE) images to identify the time sequence of the deposition of primary and secondary

hydrothermal minerals (criteria after Lamey [1961] and Ramdohr [1969]). Mineral phase compositions were determined with the electron microprobe and a Raman system.

Electron microprobe analysis of sixteen elements, BSE imaging, and X-ray mapping were obtained with the Cameca SX-50 electron microprobe in the Lunar and Planetary Laboratory at the University of Arizona. An accelerating voltage of 15 kV, sample current of 20 nA, 20 sec peak count times, and a focused (~1 μm) beam were used. We employed natural and synthetic standards and corrected the data for absorption, fluorescence, and atomic number effects using the Pouchou and Pichoir (1991) method provided with the Cameca software. The calibration standards were Crete natural albite (Na), Fo_{90} olivine USNM 111312 (Si), Boyd synthetic diopside glass (Mg), anorthite USNM 137041 (Al), synthetic MgF (F), Durango apatite (P), Penn State orthoclase 1 (K), natural wollastonite (Ca), Minas Gerais rhodonite 104791 (Mn), natural rutile (Ti), natural sodalite (Cl), Rockport fayalite (Fe), chromite USNM 117075 (Cr), Lindstrom synthetic Ni-bearing diopside glass (Ni), V metal (V), and natural barite (S).

We also analyzed selected mineral phases with a micro-Raman system equipped with a 200 mW tunable argon laser, CCD detector, and spectrograph capable of better than 1 cm^{-1} resolution at the Department of Geosciences, University of Arizona.

TIME-SPACE DEPOSITIONAL SEQUENCE

Petrographic observations allowed us to recognize the complex, selective, incomplete to pervasive, but sequential nature of the hydrothermal replacement and infiltration processes that affected the rock column at Yaxcopoil-1. Textural observations carried out at the BSE-image-scale were particularly useful. Since the studied samples are representative of different depths along the Yaxcopoil-1 hole, we were also able to establish the distribution of alteration associations in space.

In this section, we present the results of our petrographic analysis in chronologic order by following the sequence of events that affected the impactite section. First, we make an initial account of the primary mineral phases preserved in the altered protolith. Second, we identify "ground preparation" by locating high-permeability zones along the Yaxcopoil-1 borehole. Third, we distinguish pre-hydrothermal secondary phases. Fourth and fifth, we describe early and late hydrothermal minerals, their distribution with depth, and their relative introduction with respect to other phases. Finally, we assess the extent of post-hydrothermal processes.

An important goal of this part of the study was to establish the time-space depositional sequence, which allowed us to understand the mineral compositional changes determined with the electron microprobe. We present these compositional results in a subsequent section. Another goal of this part of the study was to test for the presence of a high temperature hydrothermal regime.

Throughout this report, replacement relations in time for a given mineral association are shown by plus-minus signs (±) that tie minerals. Phases that are subordinate or not always present in the temporal sequence are enclosed in parenthesis. It is important to note that these mineral associations do not necessarily represent equilibrium assemblages.

Protolith Composition

To aid in the identification of the sequence of replacement by hydrothermal products, it was important to make an initial assessment of the original mineralogy of the altered protolith because pre-existing igneous and early metasomatic mineralogies largely control the composition of subsequent secondary mineral phases.

Petrographic analyses indicate that an impact melt (unit 5) and impact melt fragments in overlying breccias at the Yaxcopoil-1 site exhibit equivalent primary mineralogies (see Kring et al. 2004). As seen through the mesh of hydrothermal alteration, unit 5 and melt fragments in the overlying breccias are composed mainly of microcrystalline clinopyroxene, plagioclase, and subordinate K-feldspar in a groundmass of possible glass, which were variably replaced by hydrothermal calc-silicates, feldspar, and phyllosilicates. Even though fresh glass does not remain, igneous clinopyroxene and plagioclase, as well as accessory phases including apatite, magnetite, ilmenite, and zircon, are well-preserved in places. Sample Yax-1_876.46, in relative terms, is the least altered. In addition to impact melt fragments, the impactite sequence also contains variably altered igneous, metamorphic, and sedimentary lithic clasts. Electron microprobe analyses revealed additional interesting compositional characteristics of the impact melt at Yaxcopoil-1, which we treat later.

Fracturing

In addition to mineralogies susceptible to hydrothermal replacement, high permeability in the host rock plays an important role in providing the channels and traps for hydrothermal fluids (i.e., Newhouse 1969). As a qualitative assessment of hydrothermal fluid controls at the Yaxcopoil-1 site, we estimated fracture densities (after the method of Titley et al. [1986] and Titley [1990]) from visual inspection of scanned color images of the Yaxcopoil-1 core. For this analysis, we considered only those fractures filled with alteration products (i.e., veins and stockworks). Thus, it was not possible to estimate the extent of pore-induced permeability from the images. The results are presented on a log scale in the third column of Fig. 1 as percentages of total rock (combined vein width in m per line-m of core). Fracture densities vary from 0 to 70%. With exception of the highly fractured unit 6 at the base of the impactite section (~885–

895 m), the highest densities occur about lithologic contacts (~820 m, ~846 m, ~858 m, and ~885 m). Correspondingly, contact zones also exhibit the most prominent hydrothermal open fracture filling (i.e., veining) and brecciation. The lowest fracture densities occur in unit 3 between 823 and 845 m. As will be seen later, this is a section in the rock column that exhibits intense hydrothermal replacement and flooding (as opposed to veining), consistent with annealing of a pre-existing high porosity zone.

Pre-Hydrothermal Modification of the Protolith

Raman analyses and crosscutting relations indicate that there are four very early, low temperature mineral phases. These phases are unevenly distributed and variably present throughout the impactite section. These are calcite, halite, gaylussite ($Na_2Ca[CO_3]_2 \cdot 5H_2O$), and gypsum, in order of abundance. The earliest halite is partially preserved as crystals in the groundmass of melt fragments (Fig. 2) and as clots in breccia matrix (see Fig. 3a). Similarly, gaylussite is present as stringers that are crosscut by later K-feldspar veins. The timing of the introduction of these minerals is consistent with modification of the impactite rock column after its deposition but before the onset of a hydrothermal regime.

Early Calc-Silicate Thermal Metamorphism and Feldspar Metasomatism

The paragraphs below describe the hydrothermal mineralogies and textures we observed in order of emplacement and from bottom to top in the impactite section.

The earliest metasomatic phase we observed is pyroxene. Limited replacement of primary augite microcrysts by (thermal metamorphic) diopside occurs in samples Yax-1_876.46 and Yax-1_872.32 in the central part of unit 5. However, diopside after augite microcrysts and larger and distinctly vein-controlled metasomatic diopside-hedenbergite crystals are present in samples Yax-1_872.32, Yax-1_841.32, Yax-1_829.56, and Yax-1_828.64 (Fig. 3b). It is important to note that recognition of replacement fronts and distinction of the compositional difference between primary augite and secondary diopside was only possible with the electron microprobe.

In unit 5 and unit 3, sparse and poorly preserved amphibole occurs after pyroxene in samples Yax-1_876.46, Yax-1_872.32, Yax-1_863.51, and Yax-1_829.56. In addition, toward the top of unit 5 and in unit 2 (sample Yax-1_821.76), we observed preserved hydrothermal amphibole crystal habits (see Fig. 3c). These sites are now largely occupied by feldspar, magnetite, and chlorite ± clay.

In contrast to unit 5, unit 3 hosts poorly developed scapolite in addition to pyroxene and amphibole. Microprobe analyses confirmed that scapolite is most abundant in sample Yax-1_828.64 toward the top of this unit. Its relative time-position in the alteration sequence, however, remains unclear. It is spatially associated with primary plagioclase and/or early halite but appears also to have developed after metasomatic feldspar.

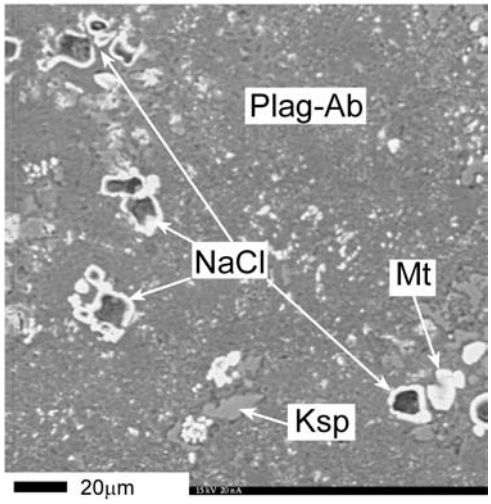

Fig. 2. Earliest halite crystals in melt fragment groundmass with albitized plagioclase and K-feldspar-magnetite alteration (Yax-1_872.32).

Compared to the limited and/or poorly preserved clinopyroxene, amphibole, and scapolite alteration (combined up to 5% by volume of rock), the distribution of feldspar metasomatism is widespread and well-developed (15 to 75 vol%) in the impactite section. Hydrothermal plagioclase is most abundant in unit 5 and unit 3, particularly in sample Yax-1_883.13 at the bottom of the former unit and in sample Yax-1_832.83 in the middle part of the latter unit. Metasomatic Na-rich plagioclase replaces primary plagioclase microcrysts (left side of Fig. 3d) and occurs as granoblasts, rims around melt clasts, and pervasive flooding in samples collected in the depth interval from 829 to 841 m.

K-feldspar alteration is observed as diffuse replacement fronts and as isolated patches. Under the microscope, it can be distinguished from plagioclase because its texture is often cloudy. A continuum of compositions, revealed by microprobe analyses, that span from K-bearing Na and Na-Ca plagioclase to K-feldspar implies that it was partially introduced along with hydrothermal plagioclase but in most instances replaced it (see Fig. 3d). Unlike hydrothermal plagioclase, K-feldspar is also vein-controlled (see Fig. 3e; dark mineral in vein is biotite ± chlorite). These (biotite) ± K-feldspar ± (quartz) ± calcite veins cut both plagioclase and K-feldspar diffuse replacement fronts, showing that they are associated with the hydrothermal event and not with post-hydrothermal processes. Much of the biotite has been converted to (chlorite) ± clay. However, it is closely associated with K-feldspar, and relict textures (less than 2 vol%) are preserved throughout unit 3. To a lesser extent, we also observed it in the immediately overlying breccia

(unit 2). In comparison with unit 3, biotite appears notably sparse in the similarly K-feldspar-altered unit 5 below. Potassium silicate metasomatism is principally abundant in sample Yax-1_857.65 in unit 4, which directly overlies the green impact melt (unit 5), and in sample Yax-1_829.56 at the top of unit 3. Thus, it is best developed directly above the two most prominent metasomatic plagioclase zones.

One interesting observation is that primary clinopyroxene microcrysts (unlike plagioclase laths) are remarkably well-preserved within plagioclase ± K-feldspar-flooded zones (see Fig. 3f). This shows that, in many instances, clinopyroxene was protected from later replacement by phyllosilicates.

Hydrothermal magnetite was introduced during feldspar metasomatism and was more closely associated in time with the K-feldspar event (see Fig. 3f). Magnetite octahedrons and replacement halos surround plagioclase laths and granoblasts, are included in K-feldspar, and are intergrown with hydrothermal quartz and pre-existing xenocrysts of shock-metamorphosed quartz. We also observed magnetite and magnetite ± (chlorite) ± clay in sites previously occupied by mafic minerals, including igneous Fe-Ti oxides. Under the microscope, hydrothermal magnetite is hard to distinguish from pre-existing igneous magnetite, and consequently, its abundance is difficult to estimate. Commonly, total magnetite does not exceed 3% of the rock volume. However, relatively larger amounts (up to 8 vol%) appear to occur in the lower parts of unit 3, below the most prominent feldspar alteration zone.

Hydrothermal apatite (see Fig. 3g) and sphene (less than 1 vol%) were introduced before and with magnetite and feldspar. They also occur after primary apatite and Fe-Ti oxides, respectively. We identified hydrothermal apatite in minor amounts throughout the impactite sequence in samples Yax-1_857.65, Yax-1_841.32, Yax-1_813.41. Sample Yax-1_872.32, in contrast, contains abundant apatite crystals in excess of 100 μm in size. These anomalously large apatites, however, reside exclusively within a clay-altered mafic clast. With the exception of sample Yax-1_872.32 in unit 5, hydrothermal sphene only occurs in unit 3 (822 to 845 m depth).

Minute and isolated crystals of chalcopyrite (primary?) are present in sample Yax-1_876.46 in unit 5. Vein-controlled magnetite ± bornite of unequivocal hydrothermal origin (see Fig. 3h), conversely, was observed in samples Yax-1_828.64 and Yax-1_821.76 about the contact between unit 3 and unit 2. Thus, sulfides associated to the hydrothermal event, albeit in trace amounts, appear to occur toward the top of the K-feldspar-rich zone that affects unit 3. Pyrite is conspicuously absent in units 1 through 5 of the impactite section.

We did not identify specular hematite in any of the samples. However, hematite pseudomorphs after magnetite (also known as martite) are present and formed after deposition of the bornite and chalcopyrite mentioned above. Complete martitization was difficult to recognize in thin section (and even with the microprobe). Its presence is only evident where it is partially developed along crystal planes of magnetite octahedrons. As a result, our abundance estimates of hydrothermal hematite are also tentative. It appears to be most dominant (up to 5 vol%) in unit 2 and less so in unit 3.

Rutile formed after primary Fe-Ti oxides, igneous and hydrothermal sphene ($CaTi[SiO_4]$ [O, OH, F]), and to a lesser extent, after secondary magnetite ± hematite. We identified rutile in the most altered part of unit 5 (sample Yax-1_872.32) and throughout the impactite section above this sample. However, it appears to be most abundant (up to 3 vol%) in the lower part of unit 3 (samples Yax-1_841.32, Yax-1_836.34, Yax-1_832.83) and toward the top of the overlying unit 2 (sample Yax-1_813.41). This depth interval encloses the intense plagioclase and sphene alteration zone.

Even though the bulk of hydrothermal calcite observed occurs as turbid late veins and open-space fillings, crosscutting relationships show that there are several generations and that at least part of it was introduced during the feldspar metasomatic stage. Early (quartz) ± magnetite ± calcite veins occur in sample Yax-1_883.13 in unit 5, early K-feldspar ± magnetite ± calcite veins (see Fig. 3i) are present in sample Yax-1_829.56 toward the top of unit 3, and a prominent calcite vein with a plagioclase ± K-feldspar envelope occurs even in sample Yax-1_800.43 in unit 1 at the top of the impactite section. This last relationship shows that the hydrothermal system developed after unit 1 was deposited.

Late Hydrothermal Phyllosilicate Replacement and Veins

In this part of the study, we sought to test whether the late-stage alteration products observed at Yaxcopoil-1 were, in part or as a whole, integral elements of the hydrothermal system. Hydrothermal products associated with the impact event were differentiated from later unrelated diagenetic or weathering products with the aid of crosscutting relations and mineral compositional zoning.

Early Ca-Na-K metasomatism is followed by an extensive late-hydrated alteration association, which largely obliterated previously deposited alteration products. This late association is composed mainly of abundant phyllosilicate replacement and veins and calcite flooding and open space fillings. Phyllosilicate alteration is embodied by very poorly preserved chlorite (confirmed with Raman analyses) and abundant clay mixtures and amorphous clays, making identification of replaced mineral phases difficult. (Chlorite) ± clay after probable glass appears pervasive in unit 5 and in much of the matrix of melt clasts in overlying breccias. The former presence of glass (up to 40 vol% [chlorite] ± clay between feldspar and clinopyroxene microcrysts) in melt and melt fragments seems evident from relict glassy, as well as schlieren and other flowed textures, seen even at the scale of a hand specimen. Thus, glass appears to have been one of the major original constituents replaced by possible chlorite and, in turn, clay. Observed under the microscope, primary

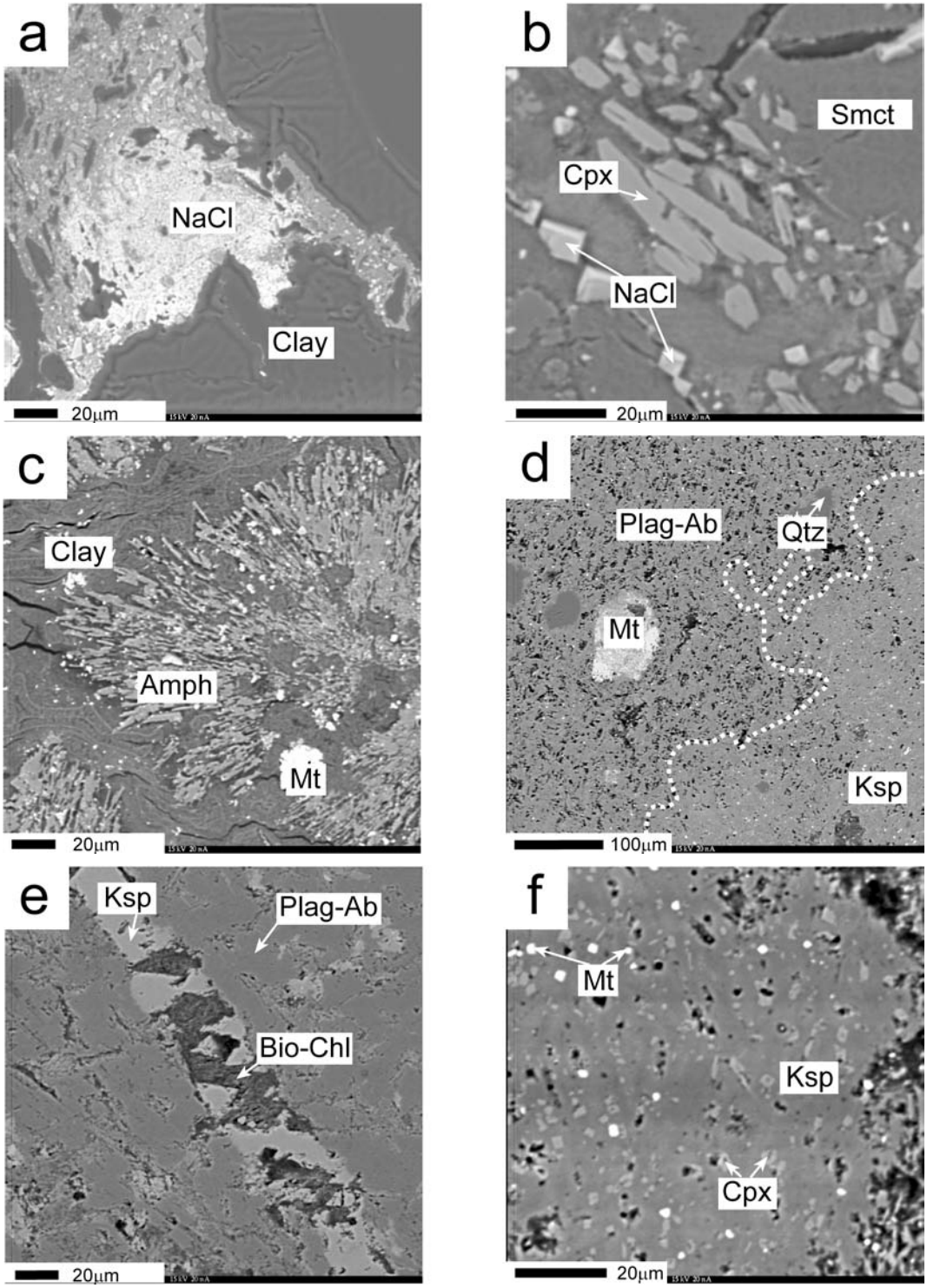

Fig. 3. Selected BSE images of hydrothermal minerals and replacement textures used for deduction of the time sequence of events: a) early salt clot in suevite breccia matrix (Yax-1_813.41); b) early diopside ± clay vein in clay-altered melt clast. Latest halite cubes along vein margin (Yax-1_872.32); c) feldspar and magnetite after relict amphibole radial habit (Yax-1_821.76); d) early plagioclase ± K-feldspar metasomatism. K-feldspar front after plagioclase ± albite (Yax-1_841.32); e) K-feldspar ± (biotite) ± chlorite vein cutting metasomatic feldspar. The dark mineral in the vein is chlorite after biotite (Yax-1_828.28); f) primary clinopyroxene preserved in secondary K-feldspar ± magnetite (Yax-1_841.32). Abbreviations: Amph = amphibole, Bio-Chl = biotite replaced by chlorite, Cpx = metasomatic diopside-hedenbergite, Ksp = metasomatic K-feldspar, Mt = magnetite, NaCl = halite; Plag-Ab = primary plagioclase replaced by secondary albite, Qtz = quartz, Smct = smectite.

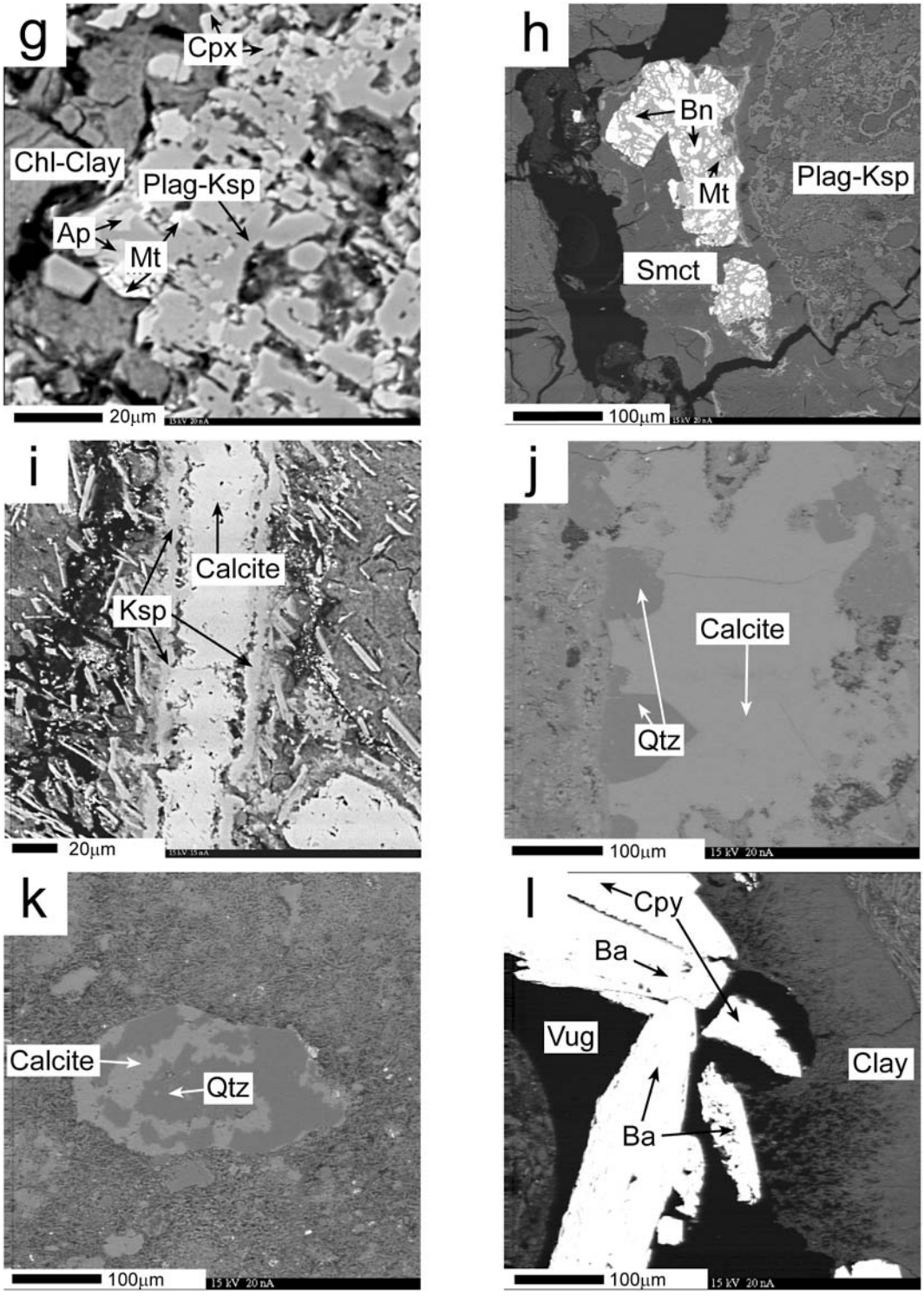

Fig. 3. *Continued.* Selected BSE images of hydrothermal minerals and replacement textures used for deduction of the time sequence of events: g) secondary clinopyroxene and feldspar ± magnetite ± apatite in (chlorite) ± clay groundmass (Yax-1_876.46); h) magnetite ± bornite vein with feldspar ± clay selvage (Yax-1_828.64); i) early K-feldspar ± calcite vein in melt fragment (Yax-1_829.56); j) late quartz and calcite vein (Yax-1_883.13); k) latest quartz- (chalcedony?) and calcite-filled vesicle (Yax-1_861.40); l) post-hydrothermal chalcopyrite ± barite in vug (Yax-1_857.65). Abbreviations: Ap = apatite, Ba = barite, Bn = bornite, Chl-Clay = chlorite replaced by clay, Cpx = metasomatic diopside-hedenbergite, Cpy = chalcopyrite, Plag-Ksp = metasomatic feldspar, Ksp = metasomatic K-feldspar, Mt = magnetite, Qtz = quartz, Smct = smectite.

minerals are also variably replaced by clay. The former presence of a mafic mineral (orthopyroxene habit?) is apparent from relict textures, particularly in samples Yax-1_876.46 and Yax-1_863.51 from unit 5 and in a melt clast in sample Yax-1_828.64 from the top of unit 3. Primary clinopyroxene and plagioclase microcrysts throughout the impactite section, however, were remarkably resistant to clay alteration. Similarly, metasomatic plagioclase and K-feldspar are only mildly affected by clay alteration. In contrast, hydrothermal pyroxene, amphibole, and biotite are rarely, if at all, preserved. An exception to the general phyllosilicate mineralogy observed throughout the impactite section occurs in sample Yax-1_841.32 at the bottom of unit 3. Here, probable epidote ± clay after feldspar is present.

The most intensely argillized samples include Yax-1_863.51 toward the top of unit 5 and Yax-1_841.32 and Yax-1_828.64 at the bottom and top of unit 3, respectively. The first sample lies between well-developed K-feldspar alteration zones, while the second and third samples envelope the most intense metasomatic feldspar zone in the impactite section. Similarly, well-developed clay alteration occurs in the lower part of unit 5 (sample Yax-1_876.46), in the top part of unit 3 (sample Yax-1_829.56), and in unit 1 (sample Yax-1_800.43). We defer clay mineralogies to the next section because we obtained constraints with the aid of the electron microprobe.

Quartz ± calcite veins (see Fig. 3j) with clay envelopes and turbid calcite filling open spaces (mainly breccia matrix) occur throughout the impactite section. They cut pre-existing clay but are also cut by (chlorite) ± clay veins. Even though it was not possible to quantify early versus late calcite abundances, much of its volume is associated with late hydrothermal stages. From bottom to top in the impactite section, calcite abundance is 3 to 5 vol% in the middle and upper parts of unit 5, decreases to 1 to 3 vol% in the overlying unit 4, but then increases substantially (with the exception of sample Yax-1_828.64) to up to 15 vol% of the rock across the highly altered unit 3 and overlying unit 2 and unit 1. Thus, secondary calcite is much more abundant in the upper half of the impactite section (excluding the carbonate-rich base of unit 6). Another exception is sample Yax-1_883.13 at the bottom of unit 5, which contains about 10 vol% calcite. This sample exhibits a second-generation breccia with angular hydrothermally altered breccia and turbid calcite clasts in a matrix of translucent calcite. This distinct second-generation breccia appears post-hydrothermal and may be tectonic (i.e., fault-related) in origin.

Post-Hydrothermal Mobilization

Several relations show that some of the minerals identified under the microscope potentially could be of post-hydrothermal origin.

Pre-existing halite crystals and clots appear to have partially recrystallized into euhedral cubes during late hydrothermal and post-hydrothermal stages (i.e., see Fig.3b). However, halite could also have been introduced anew after the hydrothermal event. Euhedral halite cubes are present in the middle part of unit 5 (sample Yax-1_872.32), the bottom of the overlying unit 4, and from the upper part of unit 3 to the top of unit 2. Halite is most abundant (up to 2 vol%) near the contact between unit 3 and the overlying suevite (sample Yax-1_821.76).

The latest clay concentrically rims vugs and other open spaces throughout the impactite sequence. Relative to earlier phyllosilicates, the distribution and abundance of this clay, however, is limited. It could have formed after the hydrothermal event during ambient-temperature diagenetic processes. Similarly, vesicles filled with calcite and quartz (chalcedony, opaline silica?; see Fig. 3k) also appear to be post-hydrothermal.

Rare late hydrothermal stringers of anatase (confirmed with the Raman survey) are preferentially within and cut particularly clay-rich zones. In addition, chalcopyrite traces occur erratically between 883 and 841 m from unit 5 to the base of unit 3. This chalcopyrite, however, crystallized with barite in open vugs and could be the product of post-hydrothermal diagenesis and/or seawater circulation (i.e., Church 1979; see Fig. 3l). Moreover, molybdenite included in clay was also found just below this contact in sample Yax-1_829.56. Vugs with barite but no chalcopyrite are also present in the upper parts of the impactite section between 829 and 813 m.

Microprobe analyses show that iron oxides in parts of the impactite section are hydrated to limonite. Partial development of limonite after magnetite and hematite occurs in sample Yax-1_863.51 close to the contact of unit 5 with the overlying breccia. More extensive hydration is evident, however, in samples between 829 and 800 m. This appears consistent with post-hydrothermal weathering of the upper parts of the impactite section. Furthermore, francolite ($Ca_5[PO_4, CO_3, OH]_3[F, Cl]$) in a calcite vein was identified with the microprobe in sample Yax-1_800.43 in unit 1. This carbonate-apatite could have formed after hydrothermal apatite as a product of weathering (McArthur et al. 1986) but could also potentially be of authigenic (phosphorite) origin (Van et al. 1990).

COMPOSITIONAL TRENDS

As in the previous section, we present the results of our electron microprobe survey in chronologic order and describe the compositional changes that we observed in early and late hydrothermal products at different levels along the core. Electron microprobe analyses of igneous and hydrothermal pyroxene, feldspar, apatite, iron oxides, as well as secondary carbonate and phyllosilicate phases support the mineralogies identified and the textural relations observed in the

petrographic analysis presented above. Compositional data allowed us to constrain, in part, some of the intensive variables (P, T, X, fO_2) from thermodynamic parameters. We include these findings in our later discussion. Overall, electron microprobe data allowed us to deduce aspects relating to the original composition of the impact melt, the initial hydrothermal solution, the nature of fluid-rock interactions, and the geochemical evolution of the fluids.

Composition of Primary Mineral Phases

Electron microprobe analyses revealed several interesting compositional characteristics of the impact melt at Yaxcopoil-1. We were able to resolve the composition of least-altered igneous clinopyroxene, plagioclase, apatite, and Fe-Ti oxides. Because the latter coexist as inclusions in primary plagioclase, they allowed us to constrain the plausible oxygen fugacity and temperature during solidification of the impact melt unit.

The composition of fresh igneous augite ($Aeg_2Fs_{11}En_{40}Wo_{46}$, on average) remains fairly constant (see Fig. 4a) in unit 5 and melt clasts in the overlying breccias. Augites contain, however, a significant fraction of aegirine (1 to 4%). Sodium in augite could only have been incorporated during primary crystallization because both primary and metasomatic clinopyroxenes were not susceptible to replacement by subsequent Na-feldspar alteration (i.e., Fig. 3f).

The freshest igneous plagioclase microcrysts also exhibit a restricted compositional range with a mean of $Or_3Ab_{43}An_{54}$. Orthoclase fractions in plagioclase vary between 0 and 7 wt%, and on average, anorthite fractions do not change significantly from unit 5 (An_{53}) to unit 2 (An_{55}) (see Fig. 4c). Given the extent of K-feldspar alteration, it was not possible to assess the abundance of primary orthoclase or sanidine.

Igneous fluorapatite ($Ca_5[PO4]_3[OH, F, Cl]$) also exhibits a noteworthy characteristic. It is unusually sulfur-rich (~2 wt% SO_3) in the bottom part of unit 5 (samples Yax-1_883.13 and Yax-1_876.46) and in the top part of unit 3 (sample Yax-1_828.64). Figure 4f shows the sulfate-silica ratios of available primary apatite analyses in the impactite section. Sulfur and silicon are known to substitute for phosphorous at the percent level in apatites of highly oxidized igneous rocks (i.e., Peng et al. 1997; Streck and Dilles 1998). We defer the implications of this to our discussion section.

Despite hydrothermal alteration, igneous Fe-Ti oxides are particularly well-preserved in unit 5. Primary magnetite in unit 5 contains a significant fraction of ülvospinel ($Usp_{31}Mt_{69}$, on average; corrected for trace element contents after Stormer [1983]). Light gray circles in Fig. 4h depict the combined concentration of trace constituents (Ti, Al, Mg, Mn, Cr, Ni, and V) in magnetite. The elevated concentrations of these trace elements (up to 0.5 atomic formula units) in unit 5 support a primary origin. In detail, Al in magnetite remains fairly constant at about 1.3 wt%. Titanium contents increase slightly from the bottom of unit 5 (~5 wt%) to the bottom of the overlying unit 4 (~8 wt%). Conversely, concentrations of magnesium (1 to 2 wt%), manganese (0.2 to 0.4 wt%), and chromium (below detection limit to about 0.1 wt%) decrease in the same depth interval. Overall, igneous magnetite is richer in trace constituents compared to hydrothermal magnetite.

Fresh ilmenite is particularly well-preserved in samples Yax-1_876.46, Yax-1_836.34, and Yax-1_813.41. Ilmenite in unit 5 (sample Yax-1_876.46) consists, on average, of $Ilm_{54}Hm_{46}$. In this sample, aluminum (0.8 wt%) and chromium (0.03 wt%; below detection limit) concentrations are comparable to those observed in primary magnetite. Magnesium (0.1 wt%) and manganese (0.05 wt%; below detection limit) contents, however, are relatively lower than those of magnetite.

From these results, it is apparent that the original compositions of the impact melt and melt clasts in overlying breccia units are equivalent, consistent with the petrographic results presented in the previous section.

Composition of Secondary Mineral Phases

Once the character of primary phases was established, we were able to better distinguish the compositional changes that took place during hydrothermal activity. Electron microprobe data provided us with an improved picture of the zoning and extent of pyroxene and feldspar metasomatism, as well as Fe, Mg, and halogen contents in hydrous phases. Compositional results further allowed us to test for the presence of post-hydrothermal weathering products at Yaxcopoil-1.

We identified diopside after augite microcrysts in unit 5 (samples Yax-1_876.46 and Yax-1_872.32) and at the base (sample Yax-1_841.32) and top (samples Yax-1_829.56 and Yax-1_828.64) of unit 3. Electron microprobe traverses across pyroxene microcrysts in a given thin section revealed irregular areas of replacement. Compared to igneous clinopyroxene, the Ca and Fe fractions of diopside ($Aeg_3Fs_{18}En_{32}Wo_{47}$, on average) from these replacement zones are significantly higher. Even more Fe-rich vein-controlled metasomatic hedenbergite ($Aeg_3Fs_{33}En_{11}Wo_{53}$) occurs toward the top of unit 3 in samples Yax-1_829.56 and Yax-1_828.64 (see Fig. 4b). However, Na concentrations in hydrothermal pyroxene remains comparable to that of primary pyroxene. The relative compositions of available analyses of primary augite (black circles) and secondary diopside and hedenbergite (gray circles) are contrasted in the pyroxene quadrilateral of Fig. 5. Table 1 gives two representative analyses of metasomatic diopside.

Incipient scapolite ($[Na, Ca, K]_4[Al_3(Al, Si)_3Si_6O_{24}][Cl, CO_3, SO_4, OH]$) alteration (after primary feldspar and halite?) is most abundant at the top of unit 3 but, in general, appears to be spatially associated with zones of more Fe-rich

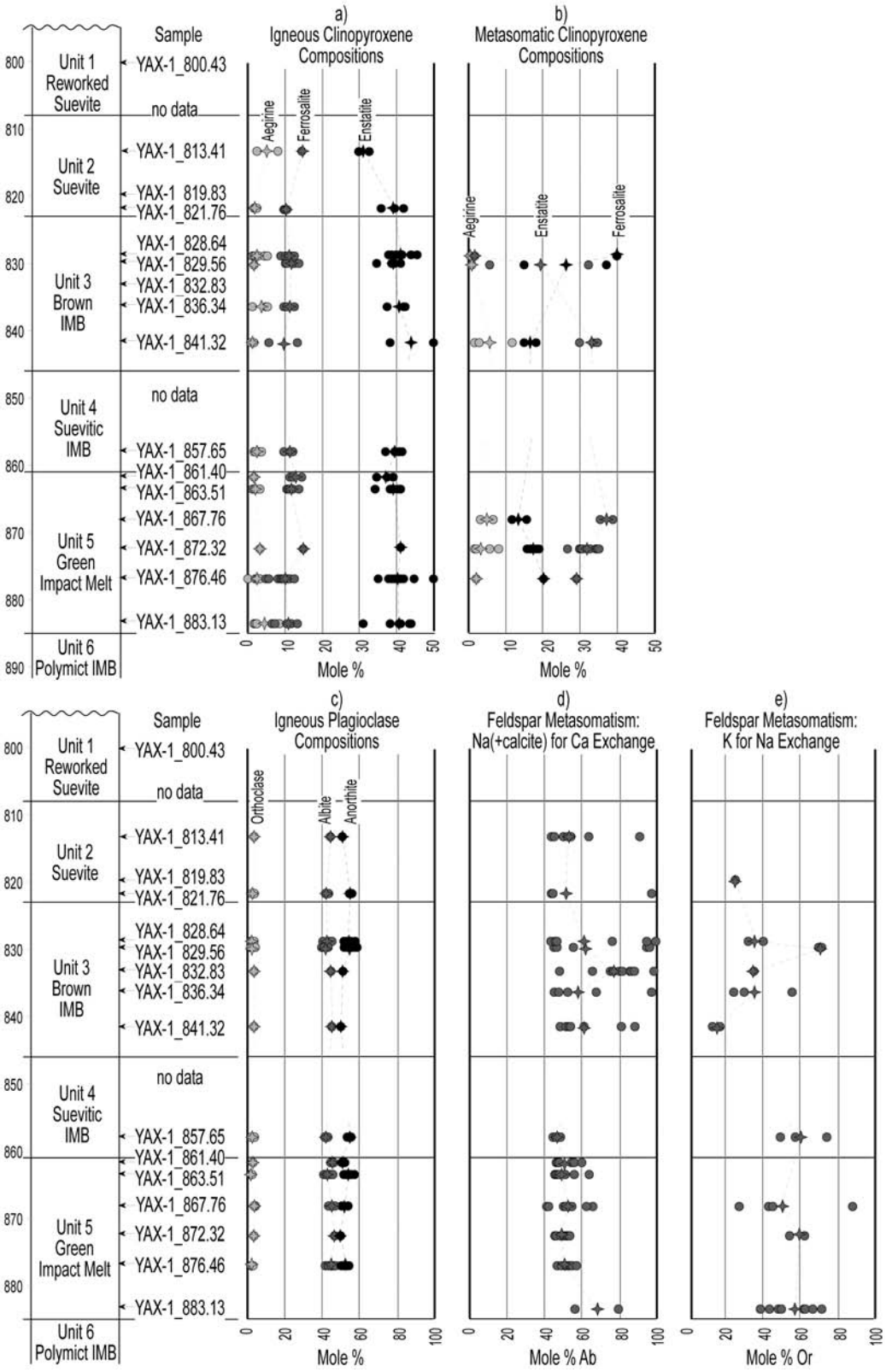

Fig. 4. Compositional changes of individual mineral phases from electron microprobe data. With depth, compositions of igneous minerals remain more or less constant compared to those of replacement minerals. Hydrothermal zoning in the Yaxcopoil-1 core is very apparent (see text for detailed explanation). The star symbols represent the average compositional changes from sample to sample.

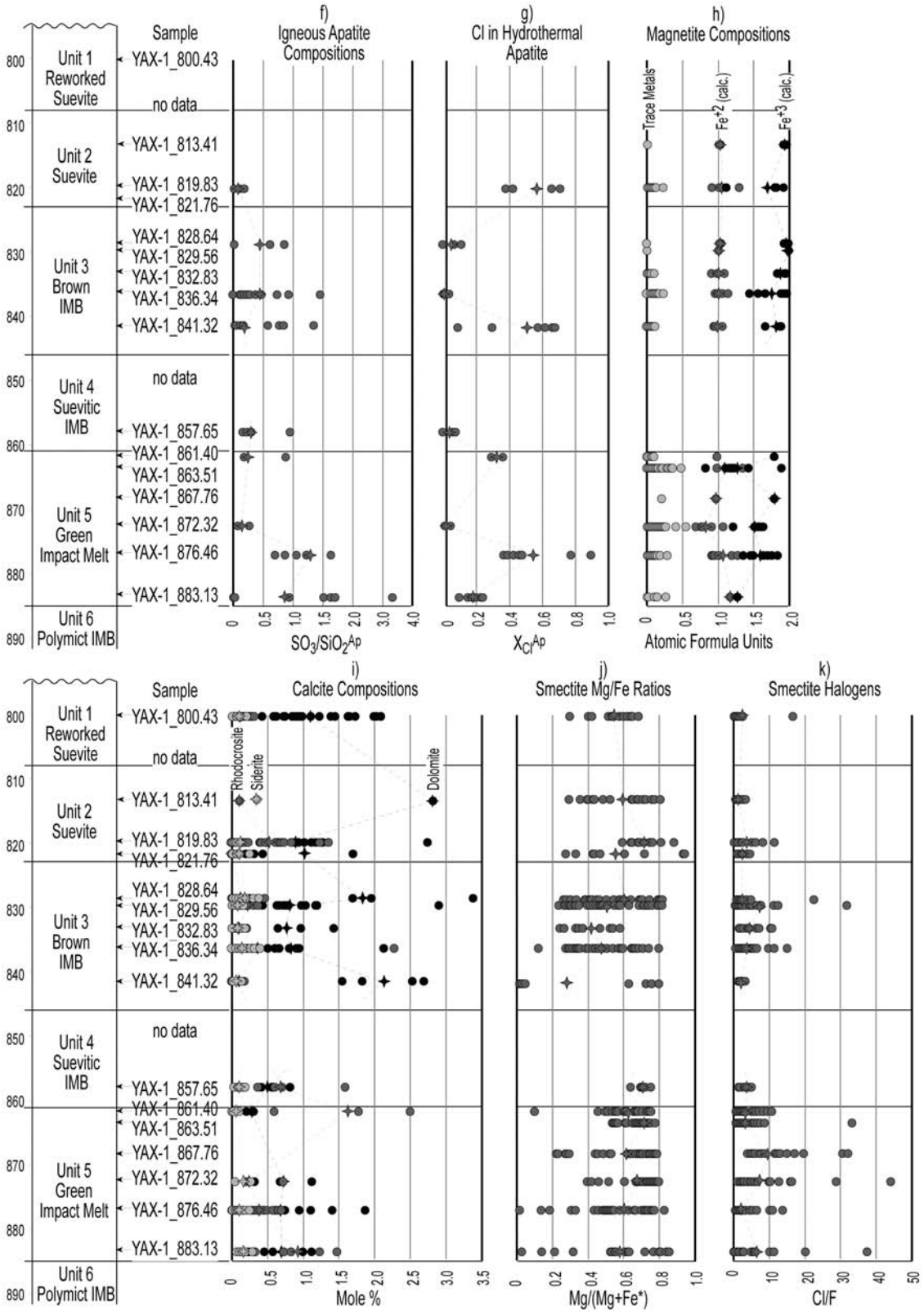

Fig. 4. *Continued.* Compositional changes of individual mineral phases from electron microprobe data. With depth, compositions of igneous minerals remain more or less constant compared to those of replacement minerals. Hydrothermal zoning in the Yaxcopoil-1 core is very apparent (see text for detailed explanation). The star symbols represent the average compositional changes from sample to sample.

metasomatic pyroxene. A representative analysis is included in Table 1.

Chlorine contents in apatite that was affected by hydrothermal activity are very low at the bottom and in the middle part of unit 5 (samples Yax-1_883.13 and Yax-1_872.32), at the bottom of unit 4 (sample (Yax-1_857.65), and in the upper half of unit 3 (samples Yax-1_829.56 and Yax-1_828.64) (see Fig. 4g). A selected apatite analysis is given in Table 1. Even though fluorine numbers are not reliable because of anisotropic diffusion during analysis (see Stormer et al. 1993), low chlorine contents in apatites coincide with the most intensely metasomatized zone in unit 3. However, Cl-poor apatite zones also occur lower in the impactite section where pyroxene and feldspar metasomatism was not as strong.

Electron microprobe results show that metasomatic alkali exchange in igneous plagioclase was extensive but occurred to variable degrees throughout the impactite section (see Table 1 for selected analyses). The best-developed Na for Ca replacement occurs at the base of unit 5 (sample Yax-1_883.13) and in units 3 and 2 (see Fig. 4d). Complete albitization of primary plagioclase occurs locally in the depth interval from 822 to 836 m and, particularly, in sample Yax-1_832.83. Albite alteration, thus, appears to envelope the most important secondary pyroxene zone. Potassium feldspar after both primary and metasomatic plagioclase is present about the lower and upper contacts of unit 5 (samples Yax-1_883.13 and Yax-1_857.65) and in the middle part of unit 3 (see Fig. 4e). This latter zone hosts the best-developed K-feldspar, which appears to have been deposited with and after the most significant albite alteration. The anorthite-orthoclase-albite diagram of Fig. 6 illustrates the continuum of variable replacement that is evident from available analyses. Black circles show igneous plagioclase, while gray circles depict metasomatic feldspar.

Available electron microprobe analyses of amphibole show that it has been pervasively replaced by clay (mostly present in unit 5; see Table 1 for representative analysis). Similarly, most of the biotite is argillized. However, the better-preserved secondary biotites (mostly present in unit 3) suggest that they are magnesian ($Phl_{52}Ann_{20}Sid_{28}$; see Table 1). Based on Fe-rich clay after biotite, however, the previous existence of a more important annite fraction in biotite cannot be precluded.

We calculated Fe^{+3} and Fe^{+2} in both primary and hydrothermal magnetite (estimation procedure after Droop [1987]) to explore iron oxidation state zoning in the altered impactite section. Only those magnetites that were not partially altered to martite and limonite were considered in this analysis. Fig. 4h illustrates the data. These estimates show that reduced iron remains more or less constant at about 1 atom formula unit (afu) through the impactite section. Oxidized iron is about 1.5 afu in the ülvospinel-bearing magnetites of unit 5. In contrast, the oxidized iron in unit 3 and overlying units

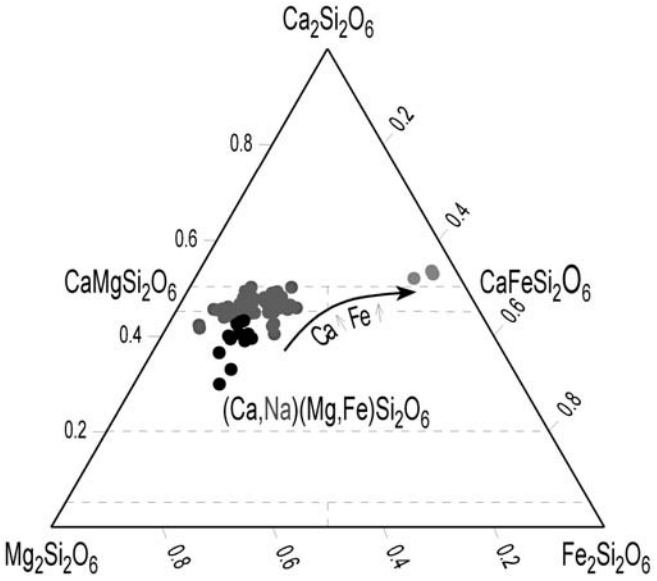

Fig. 5. Electron microprobe analyses of pyroxenes showing the compositional contrast between primary augite (black circles) and thermal metamorphic diopside and metasomatic hedenbergite (gray circles).

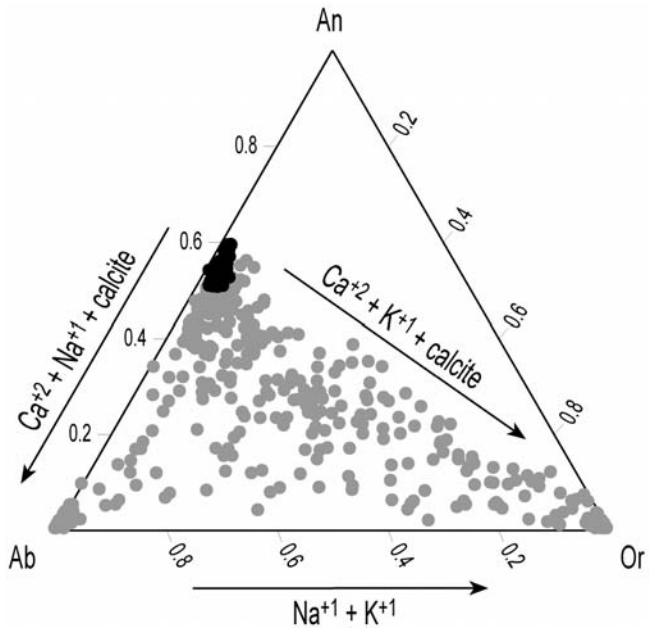

Fig. 6. Electron microprobe analyses of feldspars illustrating the great extent of metasomatic alkali exchange. Igneous plagioclases are shown in black circles.

approximates the ideal 2 afu of fairly pure hydrothermal magnetite. Even though zinc was not part of the calibration package, electron microprobe qualitative energy-dispersive spectrometry (EDS) confirmed the presence of an important zinc component in some hydrothermal magnetite grains (gahnite?) in sample Yax-1_883.13 from the bottom of unit 5.

Representative analyses of hydrothermal magnetite,

Table 1. Selected electron microprobe analyses of early hydrothermal minerals.[a]

Mineral	Clinopyroxene		Scapolite	Sphene	Apatite	Feldspar			Amphibole ± Clay	Biotite ± Clay
Sample	Yax-1	Yax-1	Yax-1	Yax-1	Yax-1	Yax-1	Yax-1	Yax-1	Yax-1	Yax-1
ID	872.32	828.64	836.34	836.34	883.13	829.56	836.34	819.83	863.51	836.34
Weight % oxide										
SiO_2	51.18	47.62	60.86	30.44	n.d.[b]	66.40	64.84	62.51	48.37	35.64
TiO_2	0.31	0.78	0.43	38.72	n.d.	n.d.	n.d.	0.48	0.25	1.60
Al_2O_3	1.02	9.28	23.20	0.79	n.d.	20.75	18.76	18.09	12.13	15.21
FeO_T	11.88	8.56	0.60	0.80	0.25	0.31	0.23	2.54	3.71	17.91
Fe_2O_{3calc}										
FeO_{calc}										
MgO	11.04	10.43	0.11	n.d.	0.10	0.15	n.d.	1.03	9.00	13.77
MnO	0.34	0.09	0.03	n.d.	0.06	n.d.	0.01	0.07	0.15	0.40
V_2O_5	n.d.		0.04	0.39	n.d.	n.d.	n.d.	n.d.	n.d.	0.25
CaO	23.37	22.65	5.41	28.53	54.10	0.77	0.03	6.76	16.99	0.03
Na_2O	0.53	0.26	5.22	0.04	0.13	11.22	0.07	3.59	3.14	0.23
K_2O	0.05	1.12	1.93	0.02	0.01	0.28	16.19	5.82	0.45	8.32
P_2O_5	0.02	0.18	0.13	0.02	39.61	n.d.	n.d.	0.28		0.01
S	0.01	0.03	0.02	n.d.	0.12	0.01	n.d.	0.02		n.d.
Cr_2O_3	n.d.		n.d.	0.05	0.01	0.01	0.03	n.d.	0.06	0.05
NiO	n.d.		n.d.	n.d.	n.d.	n.d.	n.d.	n.d.	0.09	n.d.
F	0.05	0.03	0.12	0.05	5.26[c]	n.d.	0.15	0.04	0.05	0.38
Cl	0.04	0.01	2.24	0.02	0.73	0.14	0.01	0.12	0.03	0.07
H_2O_{calc}									2.01	3.88
O = F, Cl									0.03	0.17
C			Not anal.							
Total	99.84	101.21	100.34	99.88	100.39	100.04	100.32	101.33	96.40	97.57
Atom formula units										
Si	1.94	1.76	9.04	0.99		2.91	3.00	2.85	7.09	5.60
Al^{iv}	0.05	0.24	2.96	0.01		1.07	1.00	0.97	0.91	2.41
Al^{vi}		0.16	1.10	0.02			0.03		1.19	0.41
Ti	0.01	0.02	0.05	0.95				0.02	0.03	0.19
Fe^{3+}	0.09	0.08			0.47					
Mg	0.62	0.57	0.03		0.03	0.01		0.07	1.97	3.22
Fe^{2+}	0.29	0.19	0.07	0.02		0.08	0.01	0.10	0.45	2.35
Mn	0.01				0.01				0.02	0.05
Ca	0.95	0.90	0.86	1.00	10.04	0.04		0.33	2.67	
Na	0.04	0.02	1.50		0.05	0.95	0.01	0.32	0.89	0.07
K		0.05	0.37			0.02	0.96	0.34	0.08	1.67
P					5.81					
F	0.01	0.01	0.05	0.01	2.82		0.02	0.01	0.02	0.20
Cl	0.01		0.53		0.21	0.01		0.01	0.01	0.02
S			0.01		0.11					
O basis	6.00	6.00	24.00	5.00	24.00	8.00	8.00	8.00	23.00	20.00
End members (%)										
	Aeg 2.0	Aeg 1.1				Or 1.5	Or 99.2	Or 34.3		Phl 51.7
	En 31.4	En 32.8				Ab 94.9	Ab 0.6	Ab 32.2		Ann 20.3
	Fs 18.9	Fs 15.1				An 3.6	An 0.1	An 33.5		Sid 27.9
	Wo 47.7	Wo 51.1								

[a]Abbreviations: Aeg = aegirine, En = enstatite, Fs = ferrosalite, Wo = wollastonite, Or = orthoclase, Ab = albite, An = anorthite, Usp = ülvospinel, Mt = magnetite, Ilm = ilmenite, Ht = hematite.

[b]n.d. = below detection limit.

[c]Fluorine numbers in apatite are not reliable because of anisotopic diffusion (see Stormer et al. 1993).

hematite, and rutile are given in Table 2. The Fe-Ti oxide ternary of Fig. 7 illustrates primary (black circles) and hydrothermal (gray circles) compositions. Compared to primary Fe-Ti oxides, secondary magnetite and hematite are Ti-poor. Variable replacement of magnetite by hematite (martite) and ilmenite by rutile is evident from the data, which occupy a large compositional range along a given join. Compared to primary iron oxides, these minerals also exhibit lower Al and Cr and higher V concentrations. Magnesium and Mn contents, however, appear to be equivalent in primary and secondary iron oxide phases.

Despite the fact that calculation schemes for reduced and oxidized iron contents from microprobe analyses are rough at best, results appear consistent with replacement of primary by secondary magnetite and confirm the relative location of the best-developed hydrothermal magnetite toward the top of unit 5 and in unit 3. They further point to the presence of Zn-bearing Fe-oxide toward the bottom of the impactite section.

Calcite in the impactite section contains small fractions of Mg, Mn, and Fe in decreasing order of abundance (see Fig. 4i). Even though it was not possible to differentiate early from late calcite generations with the electron microprobe, available data show that average calcite compositions change systematically around altered zones and about lithologic contacts. Average Mg contents are lowest (0.5 to 1.0 mol% dolomite) in zones where early replacement minerals formed (units 3 and 5) and highest (in excess of 3 mol% dolomite) in zones where late calcite was abundantly introduced. Manganese contents are highest (~1.5 mol% rhodocrosite) about the lower and upper contacts of unit 5 (samples Yax-1_883.13 and Yax-1_861.40) and, to a lesser extent, about the upper contact of unit 3 (sample Yax-1_819.83). Iron concentrations in calcite, in contrast, appear to remain fairly constant (less than 0.5 mol% siderite) throughout the impactite section. Even though these results are the likely sum product of multiple solution-precipitation cycles of calcite, they reveal an interesting zoning pattern.

Relict textures observed in thin section suggest that phyllosilicates pervasively replaced probable glass and variably formed after pyroxene, amphibole, biotite, and chlorite. Pyroxene is generally the best-preserved, while amphibole, biotite, and chlorite are, almost everywhere, pervasively replaced by clay. A representative analysis of clay-altered chlorite is given in Table 2. In contrast, argillization of metasomatic feldspar is minor.

Good stoichiometric electron microprobe analyses of phyllosilicates were not achieved. Even though smectite-series clays (saponite, K-montmorillonite-beidellite; see Table 2) appear to predominate, the data also point to the presence of amorphous mineral mixtures that depict the variable extent of replacement rather than mixed-layer or pure phases. Albeit limited to two dimensions, the Al versus Mg/(Mg + Fe^{tot}) diagram of Fig. 8 illustrates the compositional range apparent in analyzed phyllosilicates and explains, in part, why individual hydrous phase compositions were not effectively constrained with the electron microprobe. We used available textural relations in combination with compositional results to tentatively discriminate likely precursor phases. For reference, igneous augite and diopside-hedenbergite are shown in black and gray squares,

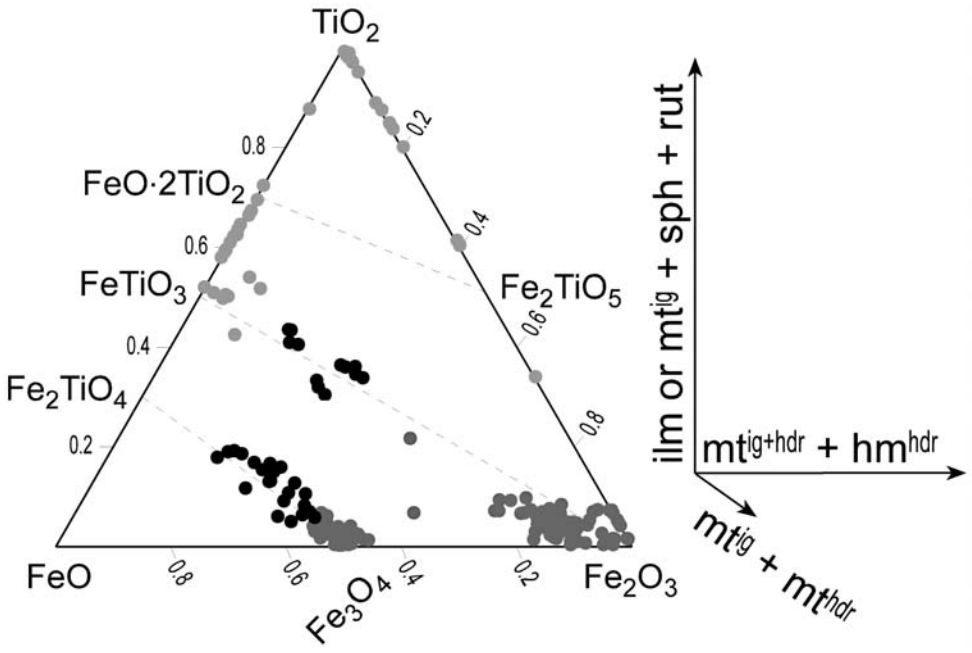

Fig. 7. Electron microprobe analyses of Fe-Ti oxides depicting primary ilmenite and magnetite compositions (black circles) and secondary magnetite, hematite (martite), and rutile compositions (gray circles). The wide range of compositions along a given join illustrate the variable degree of replacement.

Table 2. Selected electron microprobe analyses of late hydrothermal minerals and post-hydrothermal clay, limonite, and carbonate-apatite.[a]

Mineral	Magnetite	Hematite (Martite)	Rutile	Chlorite ± Clay	Saponite	K-mont-morillonite	Beidellite	Vermiculite	Limonite	Francolite
Sample	Yax-1	Yax-1	Yax-1	Yax-1	Yax-1	Yax-1	Yax-1	Yax-1	Yax-1	Yax-1
ID	841.32	813.41	883.13	813.41	863.51	863.51	800.43	876.46	828.64	800.43
Weight % oxide										
SiO_2	0.11	0.03	0.11	26.88	50.20	52.51	58.25	45.38	3.77	0.19
TiO_2	0.63	0.51	98.69	0.06	0.02	0.02	0.01	0.10	3.65	0.03
Al_2O_3	0.47	0.56	0.21	21.34	5.88	22.07	18.17	8.96	1.26	0.02
FeO_T	89.41	88.61	0.37	19.15	5.63	0.33	0.32	5.27	70.52	0.05
Fe_2O_{3calc}	66.24	98.47	0.41							
FeO_{calc}	29.80									
MgO	1.86	1.02	n.d.[b]	18.79	21.72	n.d.	0.21	15.89	1.05	0.08
MnO	0.32	0.21	n.d.	0.26	0.05	n.d.	n.d.	0.01	0.03	n.d.
V_2O_5	0.59	0.09	0.37	0.06	n.d.	n.d.	n.d.	n.d.	0.14	n.d.
CaO	0.01	0.15	0.03	0.08	0.67	7.05	1.46	0.92	0.26	56.01
Na_2O	0.05	0.02	0.02	n.d.	2.09	6.61	5.24	1.52	0.23	0.92
K_2O	n.d.	0.03	0.10	0.01	0.07	1.08	5.27	0.92	0.47	0.10
P_2O_5	n.d.	0.01	n.d.	n.d.	n.d	n.d.	n.d.	0.05		30.45
S	0.01	n.d.	0.01	n.d.	n.d	n.d.	n.d.	0.02		1.01
Cr_2O_3	0.12	0.02	n.d.	0.01	0.04	n.d.	0.01	0.01		0.04
NiO	n.d.	0.01	n.d.	n.d.	0.02	0.05	n.d	n.d.	0.06	n.d.
F	n.d.	n.d.	0.01	n.d.	0.01	n.d.	0.19	0.19	0.01	3.74[c]
Cl	n.d.	0.01	n.d.	0.01	0.33	0.01	0.22	0.19	0.05	0.09
H_2O_{calc}				11.17	15.89	9.64	8.55	19.06	18.88	
O = F, Cl					0.08		0.13	n.d.	0.01	
C										Not anal.
Total	100.23	101.15	99.96	97.82	102.53	99.38	97.79	98.37	100.39	92.72
Atom formula units										
Si				5.57	3.75	3.31	3.75	8.00	0.11	0.02
Al^{iv}	0.02	0.02		2.43	0.25	0.69	0.25		0.04	
Al^{vi}				2.79	0.26	0.96	1.12	1.86		
Ti	0.02	0.01	0.99	0.01				0.01	0.08	
Fe^{3+}	1.89	1.96	0.02	3.32	3.75	0.02	0.02	0.78	1.62	
Mg	0.10	0.04		5.81	2.42		0.02	4.18	0.05	0.01
Fe^{2+}	0.93									
Mn	0.01	0.01		0.05	0.25					
Ca				0.02	0.05	0.48	0.10	0.17	0.01	5.33
Na					0.30	0.81	0.65	0.52		0.16
K					0.05	0.09	0.43	0.21		0.01
P										2.29
F							0.04	0.10		0.85
Cl					0.04		0.02	0.06		0.01
S										0.40
O basis	4.00	3.00	2.00	32.00	10.00	10.00	10.00	24.00	3.00	10.00
End members (%)										
	X_{Usp} 1.8	X_{Ilm} 0.0		Cli 63.3						
	X_{Mt} 98.2	X_{Ht} 100.0		Cha 36.2						
	Fe_2O_3 49.9	Fe_2O_3 99.0	Fe_2O_3 0.8	Pen 0.5						
	FeO 49.2	FeO 0.0	FeO 0.0							
	TiO_2 0.9	TiO_2 1.0	TiO_2 99.2							

[a]Abbreviations: Phl = phlogopite, Ann = annite, Sid = siderophyllite, Cli = clinochlore (Mg-chlorite), Cha = chamosite (Fe-chlorite), Pen = pennantite (Mn-chlorite)

[b]n.d. = below detection limit.

[c]Fluorine numbers in francolite are not reliable because of anisotropic diffusion (see Stormer et al. 1993).

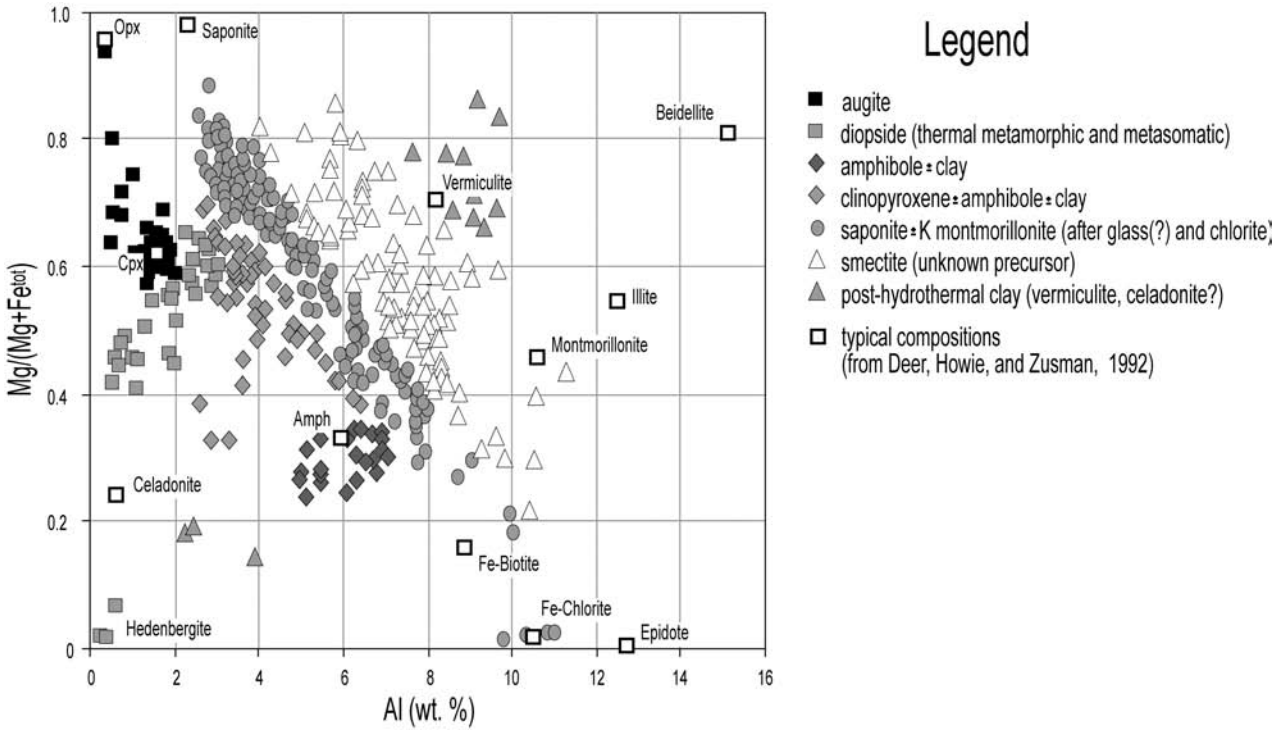

Fig. 8. Aluminum versus Mg/(Mg + Fe^{tot}) diagram of electron microprobe analyses of phyllosilicates. The compositional continuum apparent in smectite points to variable degrees of replacement. For reference, typical mineral compositions (compiled from Deer et al. [1992]) are included as white squares. Likely replacement reactions include: 1) clinopyroxene ± amphibole, 2) biotite ± illite (limited), 3) glass(?) ± chlorite ± saponite (and lesser K-montmorillonite-beidellite), and 5) post-hydrothermal clays (limited).

respectively. Dark gray and light gray diamonds correspond to amphibole ± clay and pyroxene ± amphibole ± clay analyses. Gray circles show glass(?) ± chlorite ± saponite ± montmorillonite analyses, and white triangles indicate clays for which a precursor phase was not evident. Gray triangles represent the composition of latest diagenetic(?) clays lining vugs. For reference, typical hydrous mineral compositions (compiled from Deer et al. [1992]) are included as white squares. From the diagram, it becomes apparent that, unlike other clays, smectite compositions seem to follow a systematic compositional continuum.

Magnesium-iron ratios in smectites are quite variable in a given sample and are likely inherited from the replaced precursor. On average, however, smectite Mg-Fe ratios from sample to sample (see Fig. 4j) point to Mg enrichment from the bottom to the top of unit 3 (0.3 to 0.6 Mg/[Mg + Fe^{tot}]). To a lesser extent, smectites in unit 5 exhibit the same compositional shift (0.6 to 0.7 Mg/[Mg + Fe^{tot}]). The lower Mg-Fe ratios in unit 3 generally mimic the Fe^{+3}/Fe^{+2} zoning pattern observed in magnetites from this most altered zone in the impactite section. Halogen contents in smectites are shown in Fig. 4k. The highest Cl-F ratios occur in samples Yax-1_883.13 and Yax-1_872.32 of unit 5 and in samples Yax-1_829.56 and Yax-1_828.64 of unit 3. These samples also contain apatites with the lowest Cl contents, consistent with chlorine partitioning into a fluid phase (Dilles 1987; Spear and Pyle 2002) during the late, more aqueous-dominated regime. Overall, phyllosilicate compositions in the impactite section appear to mirror the most intensely altered zones and are consistent with formation from an increasingly Fe and Cl-dominated late hydrothermal stage.

DISCUSSION

Results from this study shed further light into the original composition of the impact melt, the likely paleogeographic setting that characterized the crater before the onset of the hydrothermal regime, the composition of the hydrothermal solutions responsible for the alteration associations observed, and the processes that occurred after the hydrothermal event. Important implications were derived from the data. We discuss the significance of these in the following sections.

Petrogenesis of the Impact Melt

Consistent with previous petrologic studies (i.e., Kring and Boynton 1992; Schuraytz et al. 1994) and isotopic constraints (i.e., Blum et al. 1993; Kettrup et al. 2000), electron microprobe data from primary minerals point to a slightly alkaline andesitic composition for the original impact melt and associated melt-rich breccias at Yaxcopoil-1.

Elevated sodium contents in augite, higher-than-normal anorthite fractions in plagioclase, and important sulfur concentrations in apatite, however, give further clues as to the extent to which the melt assimilated carbonate and evaporite, besides siliceous target materials. Given the intensity of K-metasomatism, the existence of igneous K-feldspar (sanidine?) could not be positively confirmed. Conceivably, primary K-feldspar may have summed to up to one third of the total feldspar in the rock. Relict glassy textures and high Mg-Fe ratios in some smectites further suggest that the original melt contained up to 40 vol% glass and that this glass was Mg-rich. Assuming that the impact melt was emplaced under surface conditions (i.e., P = 1 bar), electron microprobe analyses of preserved coexisting primary ilmenite-magnetite pairs suggest temperatures and oxygen fugacities on the order of 760 ± 40 ºC and −15.4 ± 0.5 $\log fO_2$ units (calculated with the oxygen barometer of Spencer and Lindsley (1981), with minor component influences corrected after Stormer [1983]). The data plot in the clinopyroxene-stable field between the fayalite-magnetite-quartz (FMQ) and titanite-magnetite-quartz-hedenbergite-ilmenite (TMQHIL) buffers in $\log fO_2$-T space, consistent with the mineralogies observed. In conjunction with the microcrystalline nature of the rock, these results appear to point to the likely quenching conditions of the impact melt at Yaxcopoil-1. Because of the extent of hydrothermal alteration, the presence of primary amphibole or biotite could not be established. This hampered estimation of water saturation levels in the original melt.

Pre-Hydrothermal Paleogeographic Setting

Crosscutting relations and results from Raman spectrometry show that calcite, halite, and gaylussite were introduced shortly after the deposition of the impactite sequence. These minerals, notably gaylussite, are common low temperature evaporative concentration products in alkaline-saline lake environments (Gac et al. 1979; Li et al. 1997; Yan et al. 2002). Their presence suggests that a closed basin (or several sub-basins) akin to a volcanic caldera setting (with evaporation exceeding precipitation rates) may have formed within the Chicxulub crater before the impact-induced hydrothermal event and that the saline solutions circulated down into the impactite sequence. A more probable alternative, however, is that high-salinity formation brines derived from the evaporite-bearing target rocks below convected into the impactite section ahead of and with the impact-induced thermal front. Based on the high-salinity alteration products observed, including scapolite (i.e., Pan 1998; Johnson and Barton 2000), the most significant implication of these results is that a saline brine appears to have been largely present in the rock column before the development of the higher temperature hydrothermal regime.

Time-Space Evolution of the Impact-Induced Hydrothermal Event

The hydrothermal event at Yaxcopoil-1 evolved from an early Ca-Na-K metasomatic to a late hydrous phase-dominated stage. A summary of our petrographic and electron microprobe BSE textural observations is represented by the time-space diagram in Fig. 9. The figure shows the distribution in time and space of the hydrothermal alteration associations identified in the Yaxcopoil-1 borehole. The vertical dimension indicates space, as given by the stratigraphic section shown in the first column. The horizontal dimension represents time based on relative vein and replacement texture crosscutting relationships. Solid tie lines depict the precipitation-solution range inferred for a given alteration mineral, and short-dashed tie lines show the replacement sequence of associated alteration minerals. The long-dashed tie lines shown in the legend refer to the primary minerals replaced. Furthermore, the height of the color-coded trapezoids is a qualitative assessment of the relative abundances in space of individual hydrothermal phases. The length of the trapezoids is also a relative measure of abundance, which is a function of the amount of fluid flow through time. In addition, an attempt to show the prograde and retrograde nature of mineral associations is given by the orientation of the trapezoids. As exemplified above, many of the aspects of the dynamic evolution of the hydrothermal event could be represented.

The legend to Fig. 9 exemplifies how we reconstructed the time sequence of hydrothermal events and allows the reader to follow many of the relationships observed in each sample. For each sample, there is a set of lines representing the original phases and the associated replacement sequence. For a given sample, for instance, augite may be transformed to diopside through the effects of the early high temperature thermal metamorphic (i.e., anhydrous) stage. Clinopyroxene may then alter variably to amphibole, which, in turn, is sequentially replaced by chlorite and clay during the later fluid-dominated (i.e., hydrous) stage of the hydrothermal event. Thus, even though the sample may only contain clay, relict textures or pseudomorphs after amphibole and pyroxene reveal their former existence. Likewise, primary plagioclase microcrysts in the groundmass can partially to completely be transformed to albite and K-feldspar through metasomatic alkali exchange. Where most intense, however, the matrix may be pervasively flooded by hydrothermal feldspar, indicating filling of pre-existing pores in addition to replacement. Similarly, magnetite octahedrons may be completely replaced by hematite (martite) or only partially oxidized to hematite along cleavages. In addition, a retrograde relation in a given sample can be recognized where more than one generation of secondary mineral introduction exists. For instance, a retrograde relation would be apparent where a calcite vein with a K-feldspar selvage is cut by a K-

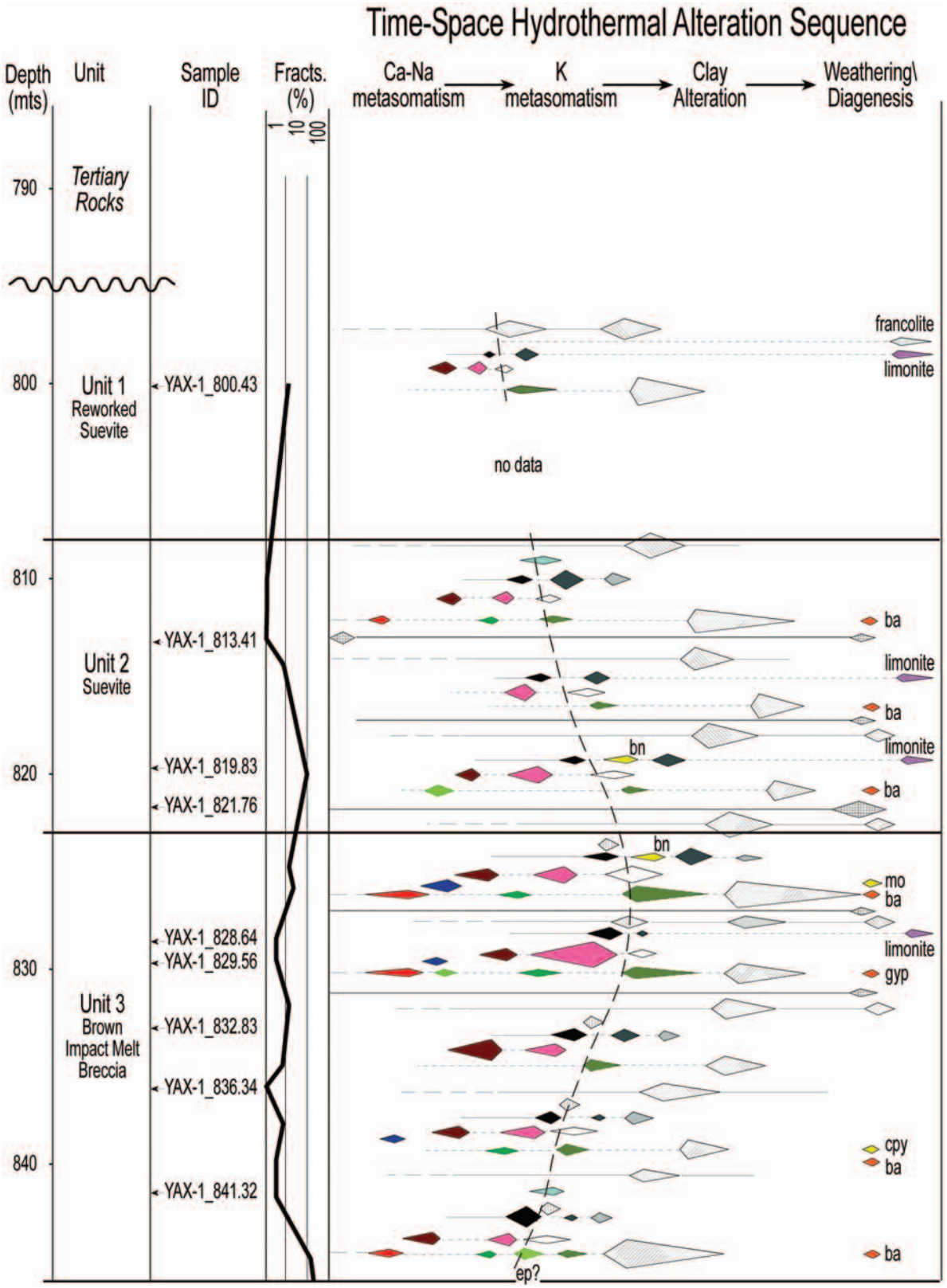

Fig. 9. Distribution of alteration associations in the impactite sequence of the Yaxcopoil-1 borehole, Chicxulub, Yucatán, Mexico. The vertical and horizontal dimensions represent the distribution in space and time, respectively (see text for detailed explanation). Abbreviations: ba = barite, bn = bornite, cpy = chalcopyrite, ep = epidote, gyp = gypsum, mo = molybdenite

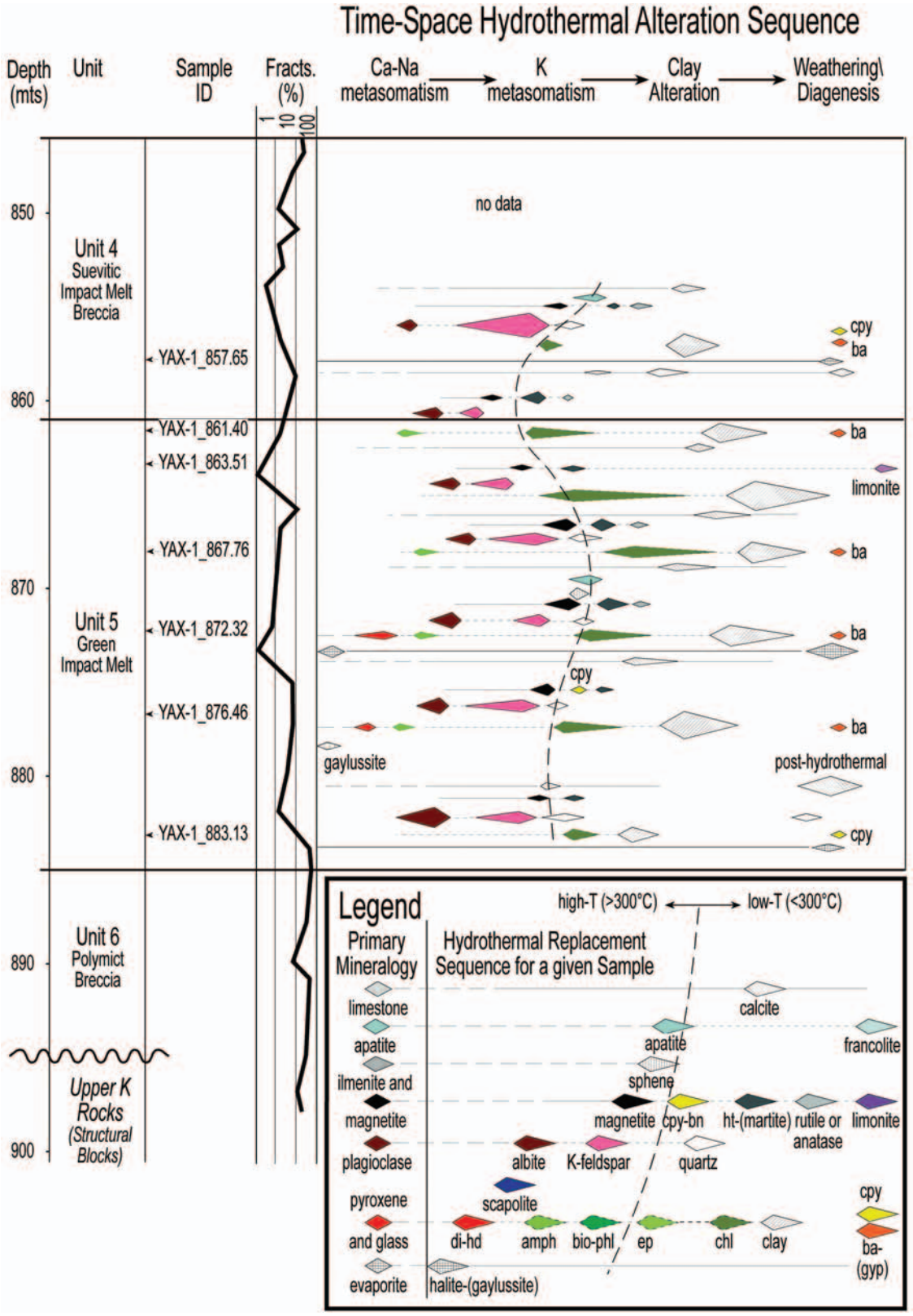

Fig. 9. *Continued.* Distribution of alteration associations in the impactite sequence of the Yaxcopoil-1 borehole, Chicxulub, Yucatán, Mexico. The vertical and horizontal dimensions represent the distribution in space and time, respectively (see text for detailed explanation). Abbreviations: ba = barite, bn = bornite, cpy = chalcopyrite, ep = epidote, gyp = gypsum, mo = molybdenite

feldspar vein with a calcite envelope. Conversely, a prograde relationship would become evident where this crosscutting relation is inverted. Likewise, barite may be identified as a product of post-hydrothermal open-space filling because it is nowhere cut by any association, and it occurs in vugs or after vesicles that are preserved.

Metasomatic hedenbergite, scapolite, sphene, and apatite present at Yaxcopoil-1 strongly suggest that the impactite section was affected by a higher temperature hydrothermal regime, which was then largely obliterated by a lower-temperature phyllosilicate- and calcite-rich overprint. Based on mineralogies and associated temperatures observed in other replacement deposits, a shape for a possible temperature gradient during the hydrothermal event at Yaxcopoil-1 can be tentatively inferred. The location of the dashed line in Fig. 9 splits hydrothermal mineral associations that typically occur above 300 °C (i.e., diopside-hedenbergite, scapolite, sphene, and apatite) from those that are commonly deposited at lower temperatures (i.e., chlorite, calcite, and clay). The between-sample projection of this temperature line suggests that unit 4 (for which, at present, we have little data), for instance, should host another highly altered zone. Similarly, the presence of high temperature alteration minerals in the upper part of the impactite sequence suggests that the hydrothermal system exhibits a sharp gradient or is cut off at the top. The later possibility could suggest a period of erosion before deposition of the Tertiary marine cover.

Origin of the Hydrothermal System

Combined petrographic and electron microprobe results confirmed the presence of metasomatic diopside-hedenbergite, scapolite, K-feldspar ± biotite in veins and magnetite with an important gahnite fraction. These minerals are common products in high temperature (>300 ºC) hydrothermal replacement environments (i.e., Arranz et al. 2002; Rosenberg et al. 2000), indicating that the rock column (and saline brine) at Yaxcopoil-1 were substantially heated. If the heat driving the hydrothermal system was directly related to cooling of the impact melt (unit 5) at Yaxcopoil-1, one would expect these alteration products to be zoned about it. However, these minerals are best developed in a high permeability zone within unit 3, some 30 m above the impact melt. To test the influence of the impact melt unit on the hydrothermal event at Yaxcopoil-1, we constructed a numerical convective heat model based on the approach used by Hanson and Barton (1989) and Barton and Hanson (1989). The model assumes a thickness of 25 m for the impact melt unit, an initial solidus temperature of 760 ºC, and wallrock at 25 ºC. Results suggest that the impact melt unit would cool down to 300 ºC in 225 yr and that the wallrock just 30 m away would remain unaffected at 25 ºC. From this calculation, it is unlikely that the high temperature hydrothermal minerals observed at Yaxcopoil-1 were a direct product of the heat released by the thin impact melt unit during its cooling, even though localized degassing of the impact melt and the overlying breccia units could have occurred. Consequently, the thermal front likely traveled from a place within the crater where the impact melt sheet was considerably thicker, implying that it took some time to arrive at the Yaxcopoil-1 site. Furthermore, heated fluids should have preferably traveled through the impactites, which were more permeable than the carbonate-dominated target rocks below.

Results from this study indicate that hydrothermal fluids within the impactite section at Yaxcopoil-1 were Cl-rich and became richer in Fe with time. In the most altered zones of the impactite section, hematite is most abundant, and Mg-Fe ratios in calcite and phyllosilicates are low. In these zones, Cl contents are low in early apatite and high in late phyllosilicates, pointing to partitioning of Cl into the hydrothermal solution. The absence of pyrite and only traces of bornite and chalcopyrite further show that the hydrothermal solution was sulfur-poor or that sulfur was flushed out of the studied section.

Crosscutting relations reveal that the hydrothermal fluid within the impactite section evolved from an initial clinopyroxene-stable to a sphene-, rutile-, and final hematite-stable oxidation state. Relative to the Ni-NiO buffer, this is a substantial oxygen fugacity shift of 4 to 5 $\log fO_2$ units, indicating that, at the higher temperatures, these fluids became more oxidized as reaction with the mafic impactite host progressed. In addition, low Mg-Fe ratios in phyllosilicates over the most altered zones may be a reflection of the higher oxidation states achieved with decreasing temperature over zones of higher fluid flow.

Even though the report on our results on samples from unit 6 in the impactite section is still under preparation, it is pertinent to mention here that the base of the impactite sequence (as well as the target rocks below) host feldspar-sulfide (as opposed to feldspar-oxide) veins and hydrocarbons. The presence of hydrocarbons is also supported by stable isotope results (Zürcher et al. Forthcoming) and fluid inclusion work by Lüders et al. (2003). These observations indicate that the initial fluid was, in fact, initially relatively reduced and that the impactite sequence was responsible for the generation of an important redox trap. The characteristic of the hydrothermal fluid at Yaxcopoil-1 appears to be analogous to one known to the ore deposits community as Fe-oxide-Cu-(Au-REE) (Barton and Johnson 1996; Johnson and Barton 2000). This is an important finding because it identifies the possible nature of the impact-related hydrothermal system at Chicxulub, and it allows comparison with other Fe-oxide hydrothermal systems and the processes and environmental settings that favor their occurrence.

Even though only minor amounts of early calcite were identified in the impactite section, geochemical considerations support the generation of calcite during the early high temperature metasomatic stage. This early calcite

could have formed from dissolution of pre-existing limestone fragments, earliest calcite in the impactite section, or carbonate target rocks but must have also been a byproduct of feldspar metasomatism. The plagioclase Na^{+1} and K^{+1} for Ca^{+2} alkali exchange reactions that form metasomatic feldspar free Ca, which commonly combines with carbon dioxide to produce calcite. Much of the Mg-, Fe-, and Mn-poor calcite is associated in space with zones that exhibit the most intense feldspar metasomatism. Although most of this calcite is not related in time with this early metasomatic event, it may have inherited its comparatively pure composition across the several down-temperature calcite precipitation-solution cycles that occurred throughout the life of the hydrothermal system.

Potassium feldspar alteration is commonly a high temperature process but has also been recognized as a product of percolation of saline brines at low temperatures (Ennis et al. 2000). Early in this study, the diffuse K-feldspar replacement fronts we observed led us to believe that feldspar metasomatism might have been a low temperature process. Crosscutting and electron microprobe relations determined since, however, established that K-feldspar is also vein-controlled and is introduced with biotite concurrently and after metasomatic plagioclase. Thus, most of the K-feldspar appears to be a product of a higher-temperature process.

With the exception of heat, it appears that all the ingredients necessary to form this hydrothermal system, including water, were available within the immediate rock volume about the Yaxcopoil-1 site before the impact.

Post-Hydrothermal Weathering

The laminated and sorted unit 1 hosts a 2 cm feldspar ± calcite vein with francolite inclusions (see Table 2 for representative analysis). This carbonate-apatite could have developed after hydrothermal apatite by weathering processes (Van et al. 1990), or it could have been incorporated as such from a phosphorite environment like those that develop in coastal marine settings, where there is a high organic matter input to sediments (Parrish 1983). Electron microprobe and Raman analyses of Fe and Ti oxides from the upper part of the impactite sequence (mainly unit 1 and unit 2) give further evidence of the presence of a weathering profile. There, magnetite and hematite have been variably oxidized to limonite (see Table 2 for selected analysis). These observations imply that the top of the impactite section was proximal to a surficial (subaerial or very shallow subaqueous) environment, where downward percolation of relatively more acid waters commonly occurs. These results may also suggest that the upper parts of both the impactite section and hydrothermal system may have been subject to some erosion before deposition of the Tertiary sedimentary cover. However, it is not known how much of the impactite section at Yaxcopoil-1 may be missing.

Post-Hydrothermal Diagenesis and Seawater Circulation

Composition and zoning of clays from the Yaxcopoil-1 core suggest that most phyllosilicates are intimately associated with the impact-induced hydrothermal event. The effects of burial metamorphism and diagenesis, as well as ocean or groundwater circulation over the last 60 Myr, appear to have been limited, based on the scarcity of the latest clays lining open spaces and vesicles in the impactite section. However, late halite cubes and calcite, chalcopyrite, and barite in vugs are plausible products of ambient-temperature diagenesis and/or seawater circulation (Church 1979; Lefticariu 2001).

CONCLUSIONS

Hydrothermal studies document not only hydrothermal aspects but also many other characteristics of the geologic record of an area. Results from this study show that:

1. Consistent with previous studies, the impact melt at Yaxcopoil-1 was derived both from assimilation of shallow target carbonate and evaporitic lithologies and from deep siliceous basement materials.
2. After deposition, the impactite sequence was permeated by a saline brine that could have percolated down into the impactite sequence but that likely originated in the evaporite-bearing target rocks below.
3. Most of the impact-induced heat appears to have been initially located elsewhere in the crater (probably about the thicker melt sheet closer to the center) and took some time to arrive at the Yaxcopoil-1 site.
4. The combined effect of pre-existing saline waters and heat produced an early high temperature (greater than 300 ºC) hydrothermal stage, which was followed by an extensive low temperature (less than 300 ºC) overprint.
5. The hydrothermal products in Yaxcopoil-1 impactites have compositional and genetic characteristics that are akin to Fe-oxide-(Cu-Au-REE) mineral deposits observed elsewhere.
6. The upper section of the hydrothermally altered impactite rock column was exposed to weathering in a subaerial and/or subaqueous setting before being covered by Tertiary marine sediments.
7. The effects of post-hydrothermal diagenesis and/or circulation of ocean water appear to have been limited.

Acknowledgments–We thank the International Continental Drilling Program, Universidad Nacional Autónoma de México, and the Chicxulub Scientific Drilling Project team for producing the Yaxcopoil-1 core. We are grateful to S. Bailey and R. Downs for the Raman analyses and M. Drake and K. Domanik for providing access to and assistance with the electron microprobe. We express our gratitude to L. Hecht and H. Newsom for thorough reviews of the manuscript and D. Stöffler for the editorial support. This paper also benefited

from an independent review by M. Barton. This work was sponsored by NSF grant EAR-0126055.

Editorial Handling—Dr. Dieter Stöffler

REFERENCES

Abramov O. and Kring D. A. 2003. Finite-difference modeling of impact induced hydrothermal systems (abstract #1359). 34th Lunar and Planetary Science Conference. CD-ROM.

Ames D. E., Dressler B., Pope K., and Pilkington M. 2003. Chicxulub impact structure hydrothermal activity (abstract #07331). Geophysical Research Abstract 5.

Ames D. E., Watkinson D. H., and Parrish R. R. 1998. Dating of a regional hydrothermal system induced by the 1850 Ma Sudbury impact event. *Geology* 26:447–450.

Arranz E., Lago M., Bastida J., and Gale C. 2002. Hydrothermal scapolite related to the contact metamorphism of the Maladeta plutonic complex, Pyrenees; Chemistry and genetic mechanisms. *Schweizerische Mineralogische und Petrographische Mitteilungen = Bulletin Suisse de Mineralogie et Petrographie* 82:101–119.

Bain J. G. and Kissin S. A. 1988. A preliminary study of fluid inclusions in shock-metamorphosed sediments at the Haughton impact structure, Devon Island, Canada. In *Papers presented at the 51st annual meeting of the Meteoritical Society.* Houston: Lunar and Planetary Institute. pp. D-7.

Barton M. D. and Johnson D. A. 1996. Evaporitic-source model for igneous-related Fe-oxide-(REE-Cu-Au-U) mineralization. *Geology* 24:259–262.

Barton M. D. and Hanson R. B. 1989. Magmatism and the development of low-pressure metamorphic belts: Implications from the western United States and thermal modeling. *Geological Society of America Bulletin* 101:1051–1065.

Blum J. D., Chamberlain C. P., Hingston M. P., Koeberl C., Marin L. E., Schuraytz B. C., and Sharpton V. L. 1993. Isotopic comparison of K/T boundary impact glass with melt rock from the Chicxulub and Manson impact structures. *Nature*:325–327.

Boer R. H., Reimold W. U., Koeberl C., and Kesler S. E. 1996. Fluid inclusion studies on drill core samples from the Manson impact crater; evidence for post-impact hydrothermal activity. In *The Manson impact structure, Iowa; Anatomy of an impact crater,* edited by Koeberl C. and Anderson R. Boulder: Geological Society of America. pp. 377–382.

Church T. M. 1979. Marine barite. In *Marine minerals.* Reviews in mineralogy 6. Washington D.C.: Mineralogical Society of America. pp 175–209.

Deer W. A., Howie R. A., and Zussman J. 1992. *An introduction to the rock-forming minerals. 2nd ed.* Harlow: Longman Scientific Technical. pp. 696.

Dilles J. H. 1987. Petrology of the Yerington Batholith, Nevada: Evidence for evolution of porphyry copper fluids. *Economic Geology* 82:1750–1789.

Dressler B. O., Sharpton V. L., Morgan J., Buffler R., Moran D., Smit J., Stoeffler D., and Urrutia J. 2003. Investigating a 65-Ma-old smoking gun; Deep drilling of the Chicxulub impact structure. *Eos Transactions* 84:125, 130.

Droop G. T. R. 1987. A general equation for estimating Fe^{+3} concentrations in ferromagnesian silicates and oxides from microprobe analyses, using stoichiometric criteria. *Mineralogical Magazine* 51:431–435.

Ennis D. J., Dunbar N. W., Campbell A. R., and Chapin C. E. 2000. The effects of K-metasomatism on the mineralogy and geochemistry of silicic ignimbrites near Socorro, New Mexico. *Chemical Geology* 167:285–312.

Gac J. Y., Al D. A., Paquet H., Fritz B., and Tardy Y. 1979. Chemical model for origin and distribution of elements in salts and brines during evaporation of waters; Application to some saline lakes of Tibesti, Chad. In *Origin and distribution of the elements,* edited by Ahrens L. H. Oxford: Pergamon Press. pp. 149–158.

Gonzalez-Partida E., Carillo C. A. and Martinez I. R. 2000. Fluid inclusions from anhydrite related to the Chicxulub Crater impact breccias, Yucatán, Mexico; Preliminary report. *International Geology Review* 42:279–288.

Grieve R. A. F. and Masaitis V. L. 1994, The economic potential of terrestrial impact craters. *International Geology Review* 36:105–151.

Hanson R. B. and Barton M. D. 1989. Thermal development of low-pressure metamorphic belts: Results from two-dimensional numerical models. *Journal of Geophysical Research* 94:10363–10377.

Hecht L., Schmitt R. T., and Wittmann A. 2003. Hydrothermal alteration of the impactites at the ICDP drill site Yax-1 (Chicxulub crater) (abstract #1583). 34th Lunar and Planetary Science Conference. CD-ROM.

Johnson D. A. and Barton M. D. 2000. Time-space development of an external brine-dominated, igneous-driven hydrothermal system; Humboldt mafic complex, western Nevada. In *Part I, Contrasting styles of intrusion-associated hydrothermal systems,* edited by Dilles J. H., Barton M. D., Johnson D. A., Proffett J. M., and Einaudi M. T. Littleton: Society of Economic Geologists.

Kettrup B., Deutsch A., Ostermann M., and Agrinier P. 2000. Chicxulub impactites: Geochemical clues to the precursor rocks. *Meteoritics & Planetary Science* 35:1229–1238.

Komor S. C., Valley J. W., and Brown P. E. 1988. Fluid-inclusion evidence for impact heating at the Siljan Ring, Sweden. *Geology* 16:711–715.

Kring D. A. 2000a. Impact events and their effect on the origin, evolution, and distribution of life. *GSA Today* 10:1–7.

Kring D. A. 2000b. Impact-induced hydrothermal activity and potential habitats for thermophilic and hyperthermophilic life. In *Catastrophic events and mass extinctions; Impacts and beyond,* edited by Koeberl C. Houston: Lunar and Planetary Institute.

Kring D. A. and Boynton W. V. 1992. Petrogenesis of an augite-bearing melt rock in the Chicxulub structure and its relationship to K/T impact spherules in Haiti. *Nature* 358:141–144.

Kring D. A., Hildebrand A. R., and Boynton W. V. 1991. The petrology of an andesitic melt rock and a polymict breccia from the interior of the Chicxulub structure, Yucatán, Mexico. In *Abstracts of papers submitted to the Twenty-second lunar and planetary science conference.* New York: Pergamon Press. pp. 755–756.

Kring D. A., Hörz F., Zürcher L. and Urrutia-Fucugauchi J. 2004. Impact lithologies and their emplacement in the Chicxulub impact crater: Initial results from the Chicxulub Scientific Drilling Project, Yaxcopoil, Mexico. *Meteoritics & Planetary Science* 39:879–897.

Lamey C. A. 1961. Contact metasomatic iron deposits of California. *Geological Society of America Bulletin* 72:669–677.

Lefticariu M. 2001. Diagenetic processes in the impact breccia and Cenozoic carbonates of the northern Yucatán Peninsula, Mexico. In *American Association of Petroleum Geologists 2001 annual meeting.* Tulsa: American Association of Petroleum Geologists and Society of Economic Paleontologists and Mineralogists.

Li J., Lowenstein T. K., and Blackburn I. R. 1997. Responses of evaporite mineralogy to inflow water sources and climate during the past 100 Kyr in Death Valley, California. *Geological Society of America Bulletin* 109:1361–1371.

Lüders V., Horsfield B., Kenkmann T., Mingram B., and Wittmann A. 2003. Hydrocarbons and aqueous fluids in Cretaceous sediments of the ICDP-Chicxulub drill core Yax-1 (abstract #1378). 34th

Lunar and Planetary Science Conference. CD-ROM.

McArthur J. M., Greensmith J. T., Benmore R. A., Hamilton P. J., Walsh J. N., Coleman M. L., and Birch G. 1986. Francolite geochemistry; Isotopic evidence for meteoric alteration on a local scale. In *Sediments down-under; 12th international sedimentological congress.* Canberra: Bureau of Mineral Resources, Geology and Geophysics. pp. 208.

McCarville P. and Crossey L. J. 1996. Post-impact hydrothermal alteration of the Manson impact structure. In *The Manson impact structure, Iowa; Anatomy of an impact crater,* edited by Koeberl C. and Anderson R. Boulder: Geological Society of America. pp. 347–376.

Newhouse W. H. 1969. *Ore deposits as related to structural features.* New York: Hafner Publishing Co. pp. 280.

Newsom H. E., Graup G., Sewards T., and Keil K. 1996. Fluidization and hydrothermal alteration of the suevite deposit at the Ries crater, West Germany, and implications for Mars. Proceedings, 17th Lunar and Planetary Science Conference. *Journal of Geophysical Research* 91:E239–E251.

Osinski G. R., Spray J. G., and Lee P. 2001. Impact-induced hydrothermal activity within the Haughton impact structure, Arctic Canada; Generation of a transient, warm, wet oasis. *Meteoritics & Planetary Science* 36:731–745.

Pan Y. 1998. Scapolite in skarn deposits; petrogenetic and geochemical significance. In *Mineralized intrusion-related skarn systems,* edited by Lentz D. R. Ottawa: Mineralogical Association of Canada. pp. 169–210.

Parrish J. T. 1983. Upwelling deposits; nature of association of organic-rich rock, chert, chalk, phosphorite, and glauconite. In *AAPG annual convention with divisions SEPM/EMD/DPA.* Tulsa: American Association of Petroleum Geologists. pp. 529.

Peng G., Luhr J. F., and McGee J. J. 1997. Factors controlling sulfur concentrations in volcanic apatite. *American Mineralogist* 82: 1210–1224.

Pevzner L. A., Kirjakov A. F., Vorontsov A. K., Masaitis V. L., Mashchak M. S., and Ivanov B. A. 1992. Vorotilovskaya drillhole; First deep drilling in the central uplift of large terrestrial impact crater. In *Abstracts of papers submitted to the Twenty-third Lunar and Planetary Science Conference.* Houston: Lunar and Planetary Science Conference. pp. 1063–1064.

Pouchou J. L. and Pichoir F. 1991. Quantitative analysis of homogeneous or stratified microvolumes applying the model "PAP." In *Electron probe quantitation,* edited by Heinrich K. F. J. and Newbury D. E. New York: Plenum Press. pp. 3175.

Ramdohr P. 1969. *The ore minerals and their intergrowths.* Oxford: Pergamon Press. pp. 1174.

Reimold W. U., Barr J. M., Grieve R. A. F., and Durrheim R. J. 1990. Geochemistry of the melt and country rocks of the Lake St. Martin impact structure, Manitoba, Canada. *Geochimica et Cosmochimica Acta* 54:2093–2111.

Rosenberg J. L., Spry P. G., Jacobson C. E., and Vokes F. M. 2000. The effects of sulfidation and oxidation during metamorphism on compositionally varied rocks adjacent to the Bleikvassli Zn-Pb-(Cu) deposit, Nordland, Norway. *Mineralium Deposita* 35:714–726.

Schuraytz B. C., Sharpton V. L., and Marin L. E. 1994. Petrology of impact-melt rocks at the Chicxulub multiring basin, Yucatán, Mexico. *Geology* 22:868–872.

Simonds C. H. and McGee P. E. 1979. Petrology of impactites from Lake St. Martin structure, Manitoba. In *Planetary interiors and surfaces,* edited by Merrill R. B., Bogard D. D., Hoerz F., McKay D. S., and Robertson P. C. New York: Pergamon Press. pp. 2493–2518.

Spear F. S. and Pyle J. M. 2002. Apatite, monazite, and xenotime in metamorphic rocks. In *Phosphates-geochemical, geobiogical, and materials importance. Reviews in Mineralogy and Geochemistry* 48:293–335.

Spencer K. J. and Lindsley D. H. 1981. A solution model for coexisting iron-titanium oxides. *American Mineralogist* 66: 1189–1201.

Stormer J. C. 1983. The effects of recalculation on estimates of temperature and oxygen fugacity from analyses of multicomponent iron-titanium oxides. *American Mineralogist* 68:586–594.

Stormer J. C., Pierson M. L., and Tacker R. C. 1993. Variation of F and Cl X-ray intensity due to anisotropic diffusion in apatite during electron microprobe analysis. *American Mineralogist* 78: 641–648.

Streck M. J. and Dilles J. H. 1998. Sulfur evolution of oxidized arc magmas as recorded in apatite from a porphyry copper batholith. *Geology* 26:523–526.

Therriault A. M., Fowler A. D., and Grieve R. A. F. 1999. The Sudbury igneous complex; Mineralogy and petrology of a differentiated impact melt sheet (abstract #1801). 30th Lunar and Planetary Science Conference.

Titley S. R. 1990. Evolution and style of fracture permeability in intrusion-centered hydrothermal systems. In *The role of fluids in crustal processes.* Washington D.C.: National Academic Press. pp. 50–63.

Titley S. R., Thompson R. C., Haynes F. M., Manske S. L., Robison L. C., and White J. L. 1986. Evolution of fractures and alteration in the Sierrita-Esperanza hydrothermal system, Pima County, Arizona. *Economic Geology* 81:343–370.

Van K. S. J., Cathcart J. B., and McClellan G. H. 1990. *Mineralogy and alteration of the phosphate deposits of Florida.* Reston: U. S. Geological Survey. pp. 46.

Versh E., Kirsimäe K., Jõeleht A., and Plado J. 2003. Impact induced hydrothermal system at Kärdla crater: Development and Biological Consequences (abstract #4120). 3rd International Conference on Large Meteorite Impacts. CD-ROM.

Yan J. P., Hinderer M., and Einsele G. 2002. Geochemical evolution of closed-basin lakes; General model and application to lakes Qinghai and Turkana. In *Lacustrine depositional systems,* edited by Tiercelin J. Amsterdam: Elsevier.

Zürcher L. and Kring D. A. 2003. Preliminary results on the post-impact hydrothermal alteration in the Yaxcopoil-1 hole, Chicxulub impact structure, Mexico (abstract #1735). 34th Lunar and Planetary Science Conference. CD-ROM.

Zürcher L., Kring D. A., Dettman D., and Rollog M. 2003. Stable isotope record of post-impact fluid activity in the Chicxulub crater as exposed by the Yaxcopoil-1 borehole (abstract #1728). 34th Lunar and Planetary Science Conference. CD-ROM.

Zürcher L., Kring D. A., Barton M. D., Dettman D., and Rollog M. Forthcoming. Stable isotope record of post-impact fluid activity in the core of the Yaxcopoil-1 borehole, Chicxulub impact structure, Mexico. GSA Special Paper.